

RESEARCH ARTICLE

Meteorology influencing springtime air quality, pollution transport, and visibility in Korea

David A. Peterson*, Edward J. Hyer*, Sang-Ok Han[†], James H. Crawford[‡], Rokjin J. Park[§], Robert Holz^{||}, Ralph E. Kuehn^{||}, Edwin Eloranta^{||}, Christoph Knote[¶], Carolyn E. Jordan^{**} and Barry L. Lefer^{††}

In an environment with many local, remote, persistent, and episodic sources of pollution, meteorology is the primary factor that drives periods of unhealthy air quality and reduced visibility. The 2016 Korea-United States Air Quality (KORUS-AQ) field study provides a unique opportunity to examine the impact of meteorology on the relative influence of local and transboundary pollution. Much of the KORUS-AQ campaign can be grouped into four distinct research periods based on observed synoptic meteorology, including a period of complex aerosol vertical profiles driven by dynamic meteorology, stagnation under a persistent anticyclone, low-level transport and haze development, and a blocking pattern. These episodes are examined using a diverse archive of ground, airborne, and satellite data. While frontal boundaries are recognized as the primary mechanism driving pollution transport in eastern Asia, results show that they are not always related to sustained periods of hazardous air quality and reduced visibility at the surface. Significant long-range transport of pollution and dust was constrained to a few short events, suggesting that the majority of pollutants sampled during KORUS-AQ originated from local sources. A severe regional pollution episode is examined in detail, featuring dense haze and significant secondary particle formation within a shallow moist boundary layer. Observations during KORUS-AQ also highlight a rapid, 40 ppbv increase in ozone pollution as a strong sea breeze front traversed the Seoul Metropolitan Area. Representativeness of meteorology and pollution conditions measured by KORUS-AQ is considered by comparison with climatology. This analysis is an essential step toward improved local and regional forecasting of air quality and visibility.

Keywords: Air quality; Pollution; Meteorology; Visibility; Pollution transport; Transboundary pollution; KORUS-AQ

1. Introduction

Air quality is a growing environmental concern in many regions across the globe. Increased populations, energy use, and industrial activity continue to generate pollutants that impact human health (e.g., Kampa and Castanas, 2008; Shang et al., 2013; Liao et al., 2017) and produce

hazardous visibility conditions (e.g., Tao et al., 2012; Fu and Chen, 2017). Over the past few decades, pollution resulting from rapid industrialization has made Eastern Asia a focal point for air quality field studies (e.g., Liu et al., 1997; Jacob et al., 2003; Liu et al., 2009; Flowers et al., 2010; Tsay et al., 2016). Understanding the factors contributing to poor air quality in this region was the primary objective of the Korea-United States Air Quality (KORUS-AQ) field study during May–June 2016 (<https://espo.nasa.gov/home/korus-aq/content/KORUS-AQ>). A variety of measurements were taken from multiple aircraft, ground sites, and ships within the territorial waters and airspace of South Korea and Japan. The broad scope of KORUS-AQ provides an unprecedented opportunity for analysis of air quality and visibility hazards arising from the combination of local and transboundary pollution.

The Korean Peninsula is an ideal location for an air quality field study due to its position along the Asian Pacific Rim. This region is known for an expansive “atmospheric brown cloud”, which is often linked to unhealthy air

* Naval Research Laboratory, Monterey, CA, US

[†] National Institute of Meteorological Sciences, Seogwipo-si, Jeju-do, KR

[‡] NASA Langley Research Center, Hampton, VA, US

[§] School of Earth and Environmental Sciences, Seoul National University, Seoul, KR

^{||} Space Science and Engineering Center, University of Wisconsin, US

[¶] Meteorological Institute, Department of Physics, LMU Munich, Munich, DE

^{**} National Institute of Aerospace, Hampton, VA, US

^{††} NASA Headquarters, Washington, DC, US

Corresponding Author: David A. Peterson
(david.peterson@nrlmry.navy.mil)

quality and poor visibility (e.g., Ramanathan et al., 2007). Development and evolution of this regional haze is driven by specific meteorology and its impact on multiple sources and species of industrial pollution (Huang et al., 2012; Fu and Chen, 2017). Eastward transport is highly correlated with mid-latitude cyclones and associated frontal boundaries (Xiao et al., 1997; Bey et al., 2001; Liu et al., 2003; Kim and Chung, 2005; Yoshitomi et al., 2011). These same disturbances influence transport of mineral dust from the Gobi and Taklamakan deserts in central Asia (Takemi and Seino, 2005; Itahashi et al., 2010; Lee et al., 2015; Chen et al., 2017; Ha et al., 2017), and facilitate heterogeneous chemical reactions with industrial pollutants (e.g., Ren et al., 2019; Wu et al., 2019). Synoptic weather patterns driving dust events can differ significantly from periods of enhanced fine particle pollution (Jung et al., 2019). Broad climate oscillations, such as El Niño/Southern Oscillation, further influence observed pollution regimes (e.g., Liu et al., 2013; Zhao et al., 2018; Jeong et al., 2018).

Transport of dust particles and industrial pollution from the Asian continent to Korea typically peaks in early to mid-spring (March–May; Liu et al., 2003; Shao and Dong, 2006). By mid-May, these impacts gradually begin to diminish. The late spring (May–June) measurement period of KORUS-AQ was selected because local pollution sources would likely play a greater role in determining observed pollution levels. Photochemical pollution also reaches a relative peak during this period (e.g., Itahashi et al., 2013). However, pollution-relevant meteorology in eastern Asia can vary significantly at both seasonal and yearly time scales (e.g., Chen et al., 1991; Zhang et al., 1997). A variety of local and transboundary pollution sources can therefore influence surface air quality at any location on the Korean Peninsula, making it effectively a crossroads of pollution in eastern Asia.

Vertical profiles of pollution are also highly dependent on local and regional meteorology. Significant variation in the depth, altitude, and composition of pollution layers has been observed across eastern Asia (e.g., Oltmans et al., 2004; Liu et al., 2011; Wong et al., 2017). Frontal boundaries are known for lifting pollution and dust particles from the boundary layer to the free troposphere (Bey et al., 2001; Liu et al., 2003). Strong mid-latitude cyclones facilitate mixing of stratospheric ozone into the troposphere (e.g., Hwang et al., 2007). Conversely, periods of stagnation often result in pollution trapped near the surface, with variation in air quality driven by localized circulations, such as the land-sea breeze (e.g., Ryu and Baik, 2013). Specific meteorology can therefore have a significant impact on the vertical structure of aerosols and trace gases, drastically impacting the extent of downwind transport and chemical evolution.

The health and safety implications of extreme pollution episodes and reduced visibility have motivated the development of comprehensive surface observation networks and modern satellite sensors capable of retrieving parameters relevant to air quality (e.g., Holben et al., 2001; Choi et al., 2018; Eck et al., 2018; Zhang et al., 2018). These observations now provide unprecedented near-real-time detection and monitoring capabilities across South Korea and other

regions of eastern Asia. A growing suite of chemical and aerosol transport modeling applications provide advanced warning of hazardous conditions (e.g., Choi et al., 2019; Lennartson et al., 2018). However, all of this technology, from the observing capability of satellites to the vertical profiles used in models, is highly dependent on meteorology.

With six weeks of detailed measurements, the KORUS-AQ campaign provides a unique opportunity to examine the key synoptic and mesoscale meteorology driving the diverse pollution regimes observed in Korea. This article provides a comprehensive overview of each pollution regime observed during the mission, ranging from periods dominated by local sources of pollution to significant long-range transport events. A variety of meteorological data, vertical profiles, and ground, airborne, and satellite observations are employed in this pursuit. Additional perspective is provided by comparing the meteorology observed during KORUS-AQ with a 30-year climatology, and considering the potential impacts on local pollution regimes from key climate oscillations that influence eastern Asia. We anticipate that this analysis will establish a foundation for improved forecasts of air quality and visibility in eastern Asia.

2. Study region and measurement strategy

The KORUS-AQ campaign was headquartered at Osan Airbase in South Korea during late spring 2016. The campaign consisted of 22 total airborne measurement days, with the first research flights conducted on 02 May and the last on 10 June. The study domain was generally bounded by the extent of South Korean airspace, but a few research flights did extend into Japanese airspace (**Figure 1**). Major ground instrumentation sites were located at Olympic Park in Seoul and the Taehwa Forest to the southeast of Seoul. Several additional ground research and operational monitoring sites were available across South Korea and Southern Japan.

KORUS-AQ employed three research aircraft, including the NASA DC-8, NASA B-200 King Air, and Hanseo University King Air. This combined fleet provided a variety of in-situ and remote sensing-based instrumentation capable of taking *in situ* measurements from the surface to altitudes above 8 km, with remote-sensing instruments looking upwards and downwards to complete the atmospheric profile. Research flights were typically coordinated between all three platforms using a variety of measurement techniques. Flight tracks for the NASA DC-8 are plotted in **Figure 1**. The NASA B-200 King Air and Hanseo University King Air followed similar flight tracks, but did not travel as far from the Korean Peninsula. Vertical profiling was conducted by the DC-8 in the vicinity of the Olympic Park and Taehwa sites during the morning, afternoon, and evening of most flight days to examine diurnal variation in pollution. Several research flights were designed to coincide with observations taken onboard two research ships operating in Korean waters as part of the concurrent Korea-United States Ocean Color (KORUS-OC) expedition (GEO-CAPE, 2015). Full details of the KORUS-AQ mission and measurement strategy are provided by Crawford (manuscript in preparation).

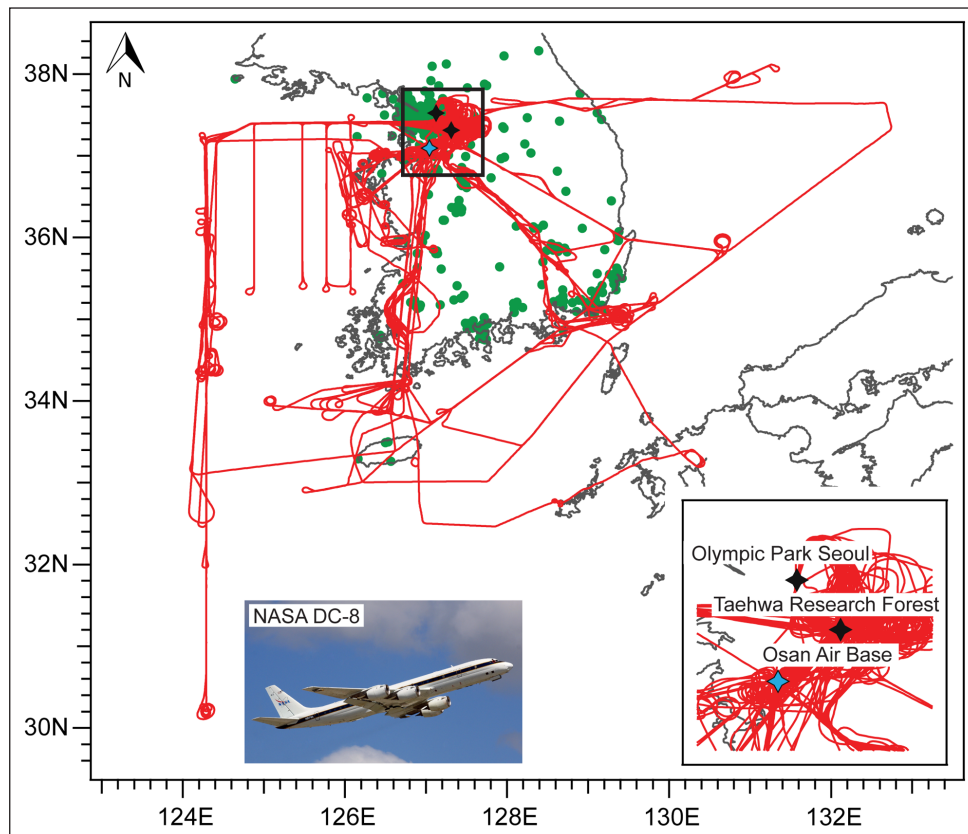


Figure 1: KORUS-AQ study region map. All flights were conducted from Osan Air Base (blue marker). Red lines denote flight tracks for the NASA DC-8. The other aircraft followed similar flight tracks, but did not travel as far from the Korean Peninsula. Olympic Park and the Taehwa Research Forest (black markers) represent the two major ground instrumentation sites, which were overflown routinely by KORUS-AQ aircraft. Green dots represent the locations of AirKorea surface pollution monitors. DOI: <https://doi.org/10.1525/elementa.395.f1>

3. General meteorology and observed pollution

The climate of South Korea is temperate, featuring four distinct seasons of winter, spring, summer and fall. Rainfall is heaviest during July and August, with surface temperatures often exceeding 30°C. The winter season of December to February is the driest, with temperatures often falling below freezing.

The polar jet stream serves as the primary storm track (westerly), influencing the development, progression, and intensity of mid-latitude cyclones and associated frontal boundaries (Figure 2). By mid-spring, disturbances associated with the polar jet often pass directly over the Korean Peninsula, influencing transport of dust, wildfire smoke, and industrial pollution (e.g., Liu et al., 2003; Lee et al., 2005; Shao and Dong, 2006; Lee et al., 2015; Fromm et al., 2016). During the late-spring (May–June) measurement period of KORUS-AQ, the polar jet stream remained the most dominant feature affecting Korean synoptic meteorology, but its position and intensity was highly variable, especially over the Asian continent.

An intensifying polar jet stream was observed over the Pacific Ocean during the second half of KORUS-AQ (25 May to 10 June), associated with the temperature gradient induced by the northward migration of the East Asian Monsoon (Sampe and Xie, 2010). The low-level boundary between the warm and moist monsoonal air mass and cooler/drier mid-latitude air masses is very

distinct in late spring, often referred to as “Meiyu” in China, “Baiu” in Japan, and “Changma” in Korea (Ding and Chan, 2005; Sampe and Xie, 2010; Lee et al., 2017). This monsoon boundary (e.g., Meiyu-Baiu or Changma Front) is evidenced by a quasi-stationary band of convective clouds and thunderstorms, slowly approaching Korea from the south (Figure 2). The monsoon boundary typically reaches the Korean Peninsula in July, well after the KORUS-AQ measurement period. However, the associated increase in observed rainfall did reach the southern portion of the study region by early June 2016, south of Jeju Island (Figure 1). Rainy periods were driven by disturbances migrating along the monsoonal boundary (e.g., Ding and Chan, 2005), which effectively served as a secondary storm track near the end of the campaign.

The synoptic features highlighted in Figure 2 set the stage for regional and localized pollution regimes, including periods of reduced visibility (e.g., Demuzere et al., 2009; Kim et al., 2014; Zheng et al., 2015; Liao et al., 2017). When considering observed synoptic meteorology, much of the KORUS-AQ campaign can be grouped into four distinct research periods:

1. Dynamic meteorology and complex aerosol vertical profiles (01–16 May);
2. Stagnation under a persistent anticyclone (17–22 May);

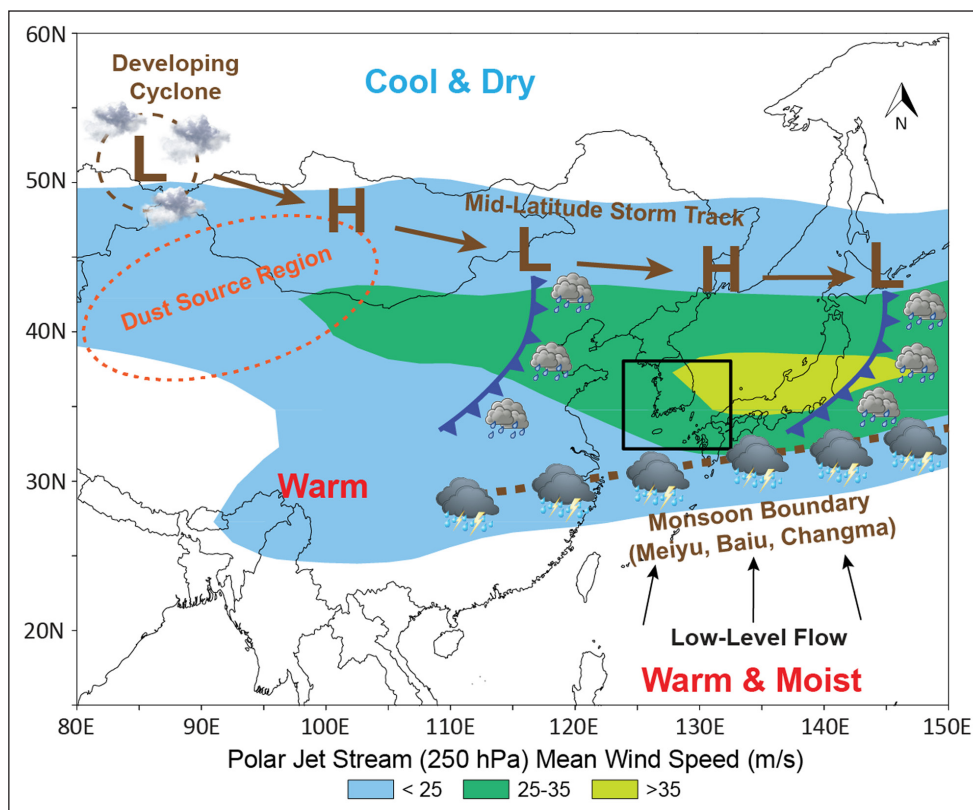


Figure 2: Schematic describing the key features that drive Korean meteorology in late spring. Shading indicates the mean position of the westerly polar jet stream (upper-level, 250 hPa) derived from wind speeds averaged over the entire KORUS-AQ measurement period (01 May–10 June 2016; NCEP–NCAR meteorological reanalysis). Brown symbols indicate important low-level features. Primary dust source regions (Gobi and Taklamakan deserts) are denoted by a dashed orange circle. Black box indicates the approximate KORUS-AQ study region (Figure 1). The location of each atmospheric component in this diagram varies. DOI: <https://doi.org/10.1525/elementa.395.f2>

3. Dynamic meteorology, low-level transport, and haze development (25–31 May);
4. Blocking pattern (01–07 June).

Figure 3 provides a time series of the distributions of ozone and atmospheric particulate matter with a diameter of less than $2.5 \mu\text{m}$ ($\text{PM}_{2.5}$) observed at AirKorea surface monitors (**Figure 1**, green dots; AirKorea, 2018) across the study region for the duration of KORUS-AQ. While ozone pollution frequently exceeded the Korean eight-hourly air quality standard of 60 ppbv, the 24-hour $\text{PM}_{2.5}$ standard of $50 \mu\text{g}/\text{m}^3$ was only exceeded during a few distinct periods. This variation is a direct result of observed synoptic and mesoscale meteorology. Subsequent discussion highlights the meteorology associated with each research period in detail.

4. The role of cold fronts in surface air quality

Cold fronts have long been recognized as the primary mechanism for episodic periods of pollution transport/export from the Asian mainland to the Pacific Ocean (Xiao et al., 1997; Bey et al., 2001; Fuelberg et al., 2003; Liu et al., 2003; Kim and Chung, 2005; Yoshitomi et al., 2011). Previous field campaigns have shown that pollution is frequently lifted above the boundary layer ahead of cold fronts, while the post frontal air mass can facilitate low-level westerly transport (e.g., Bey et al., 2001; Liu et al., 2003). However, observations during the KORUS-AQ measurement period reveal

that a specific synoptic environment is required for cold fronts to induce persistent air quality and visibility impacts at the surface.

Five out of the ten significant frontal boundaries observed during KORUS-AQ (50%) passed through the study region during the first two weeks of the campaign (**Figure 3**), which featured dynamic synoptic meteorology typical of mid-spring in eastern Asia (Chen et al., 1991, Takemi and Seino, 2005). Dynamic meteorology was also observed during the fourth week of KORUS-AQ (25–31 May), allowing four additional cold fronts to reach the study region. While these periods were each characterized by a relatively active storm track, surface air quality and visibility impacts were much more severe during the second dynamic period of 25–31 May (**Figure 3**). This disparity was driven by the relative strength of surface frontal boundaries, which is controlled by the available dynamic forcing.

Figure 4a displays the mean 250 hPa heights and wind speeds (upper-troposphere) during the initial period of dynamic meteorology from the National Center for Environmental Prediction and National Center for Atmospheric Research (NCEP/NCAR) meteorological reanalysis dataset, revealing that a relatively strong polar jet stream (averaging 35 ms^{-1} , 68 kt) was frequently positioned near the study region, supporting progressive storm movement. The polar jet also persisted along the

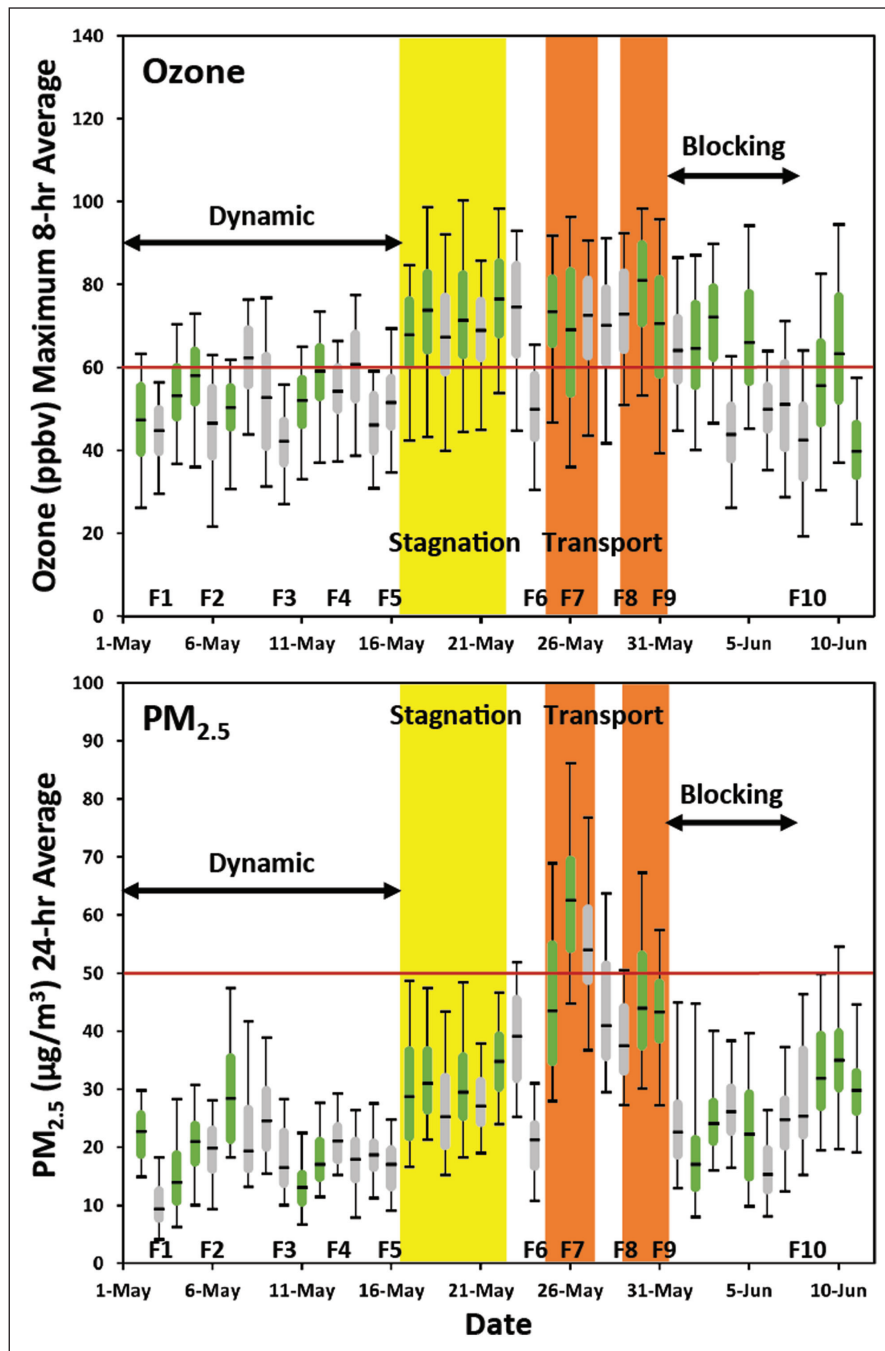


Figure 3: Distributions of ozone and $PM_{2.5}$ across South Korea during KORUS-AQ. Distributions of ozone (top) and $PM_{2.5}$ (bottom) from AirKorea surface monitors across South Korea (Figure 1, green dots) during the KORUS-AQ field study period of 01 May to 10 June 2016. The boxes are bounded by the 25th and 75th percentiles, with the median indicated as a line bisecting each box. Whiskers indicate the 5th and 95th percentiles. Days of airborne data collection are highlighted in green. Red lines denote Korean air quality standards. Periods of stagnation and sustained low-level pollution transport are highlighted in yellow and orange, respectively. The primary dynamic period and blocking pattern are denoted by black arrows. Cold front passages are numbered sequentially (Fi) at the bottom of each image. DOI: <https://doi.org/10.1525/elementa.395.f3>

border between China and Mongolia, allowing transient upper-level disturbances to induce vertical motion in a region known for prolific low-level cyclogenesis during the spring (Chen et al., 1991). Several mid-latitude cyclones developed over this region, and approached Korea from the west (Figure 4a, dark red arrows). These systems were each associated with relatively strong surface frontal boundaries that induced rapid changes in observed

surface weather conditions, resulting in short cycles between localized pollution, dust transport, rainy, and clear/clean conditions. Unhealthy pollution was therefore unable to persist, and was frequently lifted above the surface, producing complex vertical profiles of pollution. AirKorea ground sites observed some of the lowest ozone and $PM_{2.5}$ levels during this first dynamic period of KORUS-AQ (Figure 3).

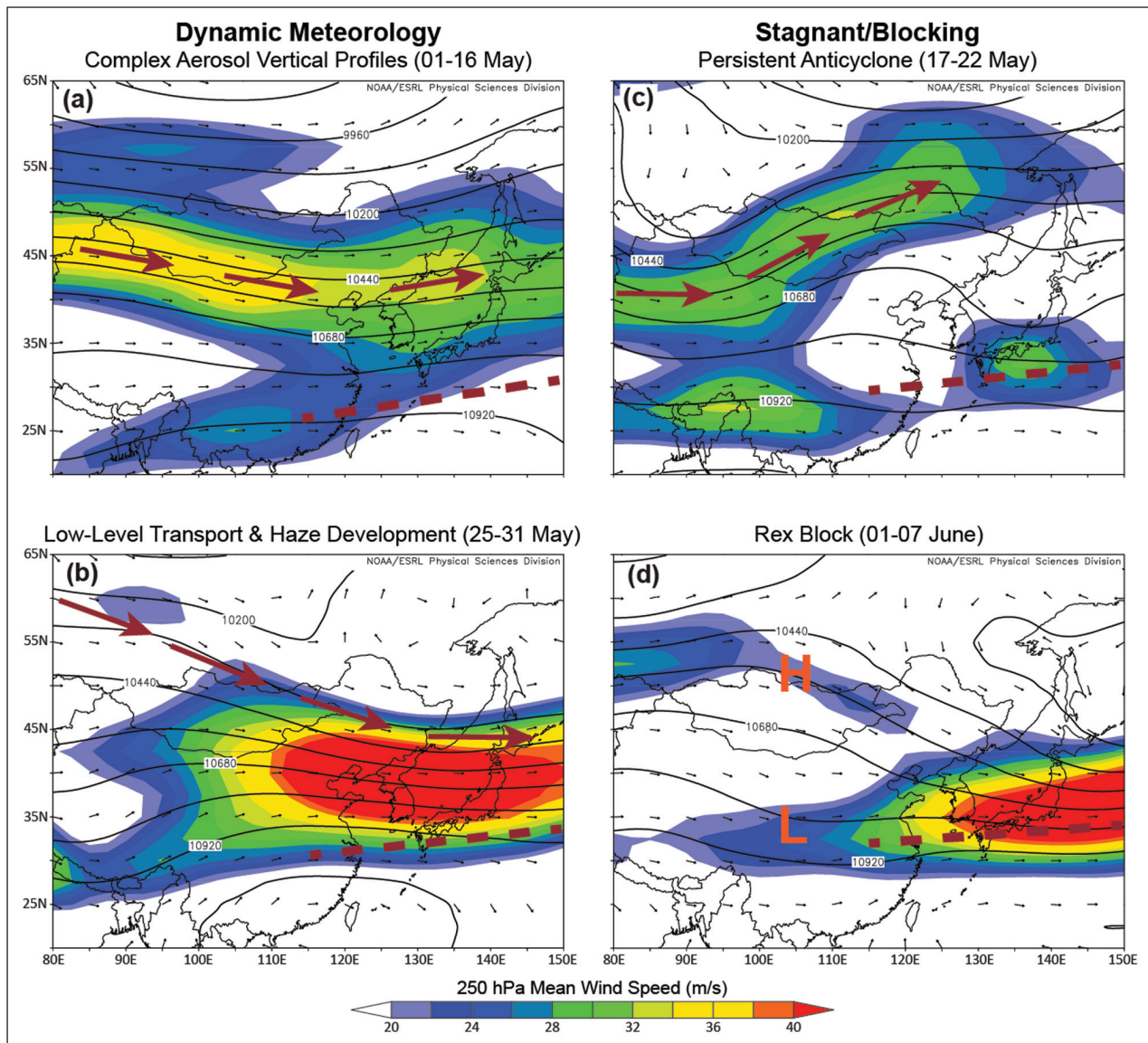


Figure 4: Average synoptic meteorology for the four research periods of KORUS-AQ. Left panels coincide with dynamic conditions and right panels coincide with stagnant or blocking conditions. The polar jet stream is displayed as 250 hPa wind speed (shaded), vectors, and heights (black contours) averaged over each KORUS-AQ research period (NCEP–NCAR meteorological reanalysis). Brown arrows and dashed brown line indicate the mean position of the low-level mid-latitude storm track and the monsoon boundary (e.g., Meiyu, Baiu, Changma Front), respectively. DOI: <https://doi.org/10.1525/elementa.395.f4>

In contrast, the second period of dynamic meteorology (25–31 May) featured a significantly weaker polar jet stream over central Asia (**Figure 4b**). The mid-latitude storm track was displaced to the north of the study region, while the low-level monsoon boundary continued to approach from the south. These conditions resulted in comparatively weaker frontal boundaries affecting the study region and slower progression. Vertical motion was reduced, favoring sustained low-level westerly transport and secondary particle formation induced by both local and distant sources. This period therefore coincided with the most unhealthy ozone and PM_{2.5} levels observed at the surface during KORUS-AQ (**Figure 3**). Details of these contrasting pollution regimes are provided in the following sections.

5. Dynamic meteorology and complex aerosol vertical profiles

While sustained surface air quality impacts were absent, the early dynamic period of KORUS-AQ featured the most complex vertical profiles of aerosol particles and trace gasses observed during the campaign. The coincidence of a strong jet stream and associated cyclogenesis over the primary dust source regions of central Asia (Gobi and Taklamakan deserts, **Figures 2, 4a**) was ideal for initiating expansive springtime dust storms (e.g., Takemi and Seino, 2005; Liu et al., 2010). As mid-latitude cyclones developed and strengthened over these regions, increasing surface winds began the process of lofting dust particles into the atmosphere, especially along the southern and western sides of the circulation (Takemi and Seino, 2005).

Figure 5a–d provides true color imagery from the Advanced Himawari Imager (AHI) onboard the Himawari-8 Satellite. This display highlights two strong mid-latitude cyclones that developed over central Asia, traversed the primary dust source regions, and affected Korea during 03–06 May. An expansive dust plume was associated with the second cyclone as it approached Korea on 05–06 May (**Figure 5c, d**). Over time, these airborne dust plumes encountered large-scale lifting mechanisms associated with the broader storm system, including distinct

frontal boundaries and the expansive warm conveyor belt (Eckhardt et al., 2004; Itahashi et al., 2010; Fromm et al., 2016). These processes ultimately lofted dust particles over a broad range of altitudes, facilitating transport to Korea. However, as each storm system passed over the industrialized regions of northern China, the same lifting mechanisms enabled other forms of pollution to reach similar altitudes (e.g. Shin et al., 2015; Lamb et al., 2018), facilitating heterogeneous chemical reactions (e.g., Ren et al., 2019; Wu et al., 2019).

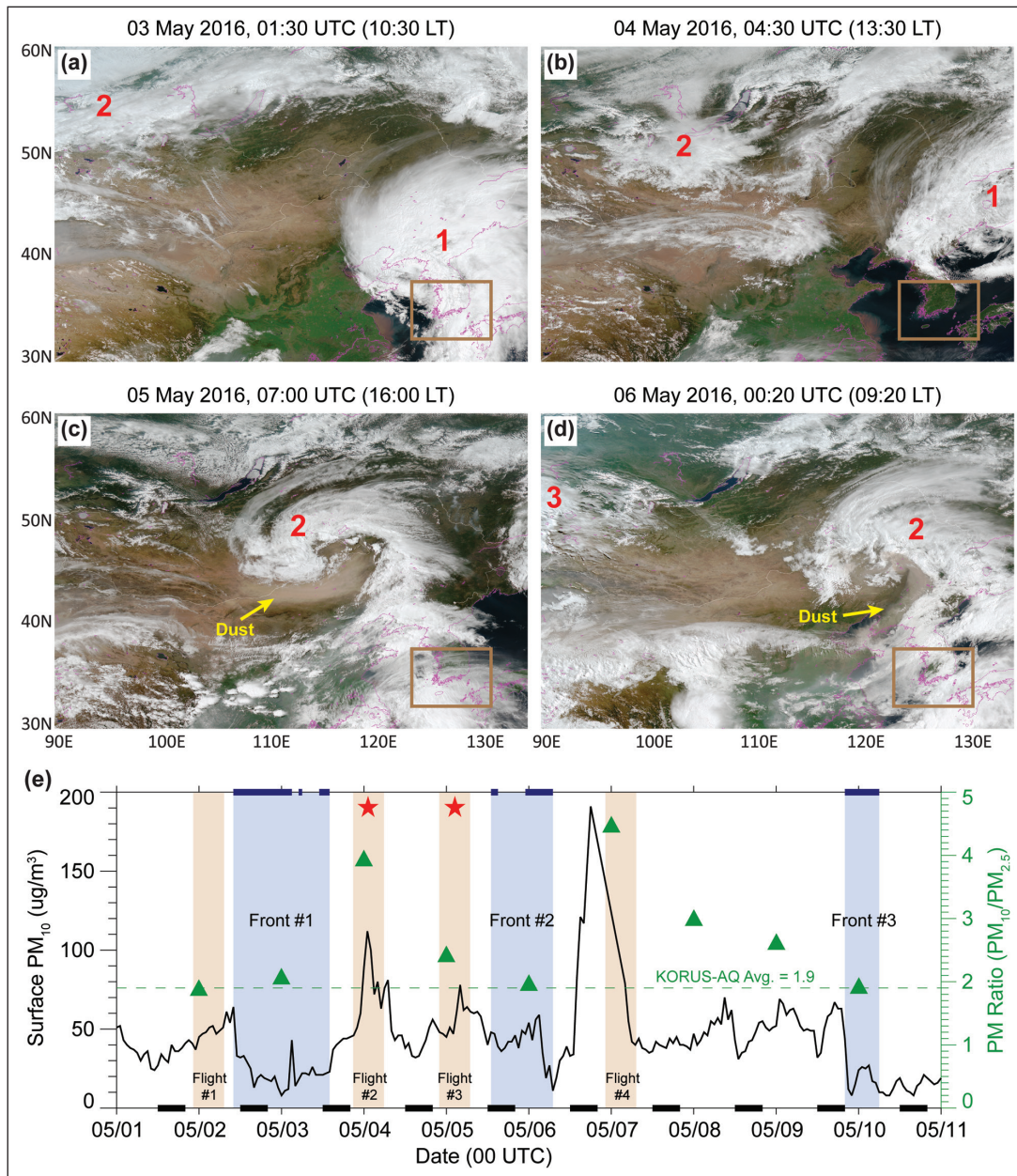


Figure 5: Large dynamic forcing, dust transport, and ensuing surface impacts. AHI true color imagery for 03–06 May 2016 (**a–d**), highlighting dynamic meteorology and dust transport. Storm systems/frontal boundaries are numbered sequentially. Brown box indicates the approximate KORUS-AQ study domain. A complete time series of PM_{10} (black) and PM ratio ($PM_{10}/PM_{2.5}$, green) is provided in (**e**) for an observing station located in Seoul (#108: 37.5714°N, 126.9658°E). Cold front passages are highlighted in light blue, with periods of precipitation indicated by a solid blue bar on the upper x-axis. Beige shading indicates the approximate duration of each NASA DC-8 science flight. Black bars on the bottom x-axis indicate nighttime periods (12:00–20:00 UTC, 21:00–05:00 LT). Red stars coincide with dust particles mixing to surface in Figure 6. DOI: <https://doi.org/10.1525/elementa.395.f5>

Complex layering of aerosol particles was a frequent occurrence during the early dynamic period of KORUS-AQ, especially between 04 and 07 May. **Figure 6** provides an example vertical profile from 04 and 05 May via the ground-based High Spectral Resolution Lidar (HSRL) located in Seoul (University of Wisconsin, 2019), which was deployed by NASA during KORUS-AQ. The HSRL provides separation between the molecular background and particulate (cloud and aerosol) scattering with very high signal to noise. This capability provides direct measurements of the particulate backscatter cross-section and depolarization at a wavelength of 532 nm. The system also provides attenuated backscatter at 1064 nm, facilitating observations of aerosol vertical profiles and cloud properties.

During 04–05 May, Korea was positioned between the two mid-latitude cyclones highlighted in **Figure 5a, b**, with one passing on 03 May and second approaching from the west. HSRL backscatter data highlight several layers of aerosol between the surface and 8.0 km above ground level (AGL), especially during the nighttime period of 04 May and the morning hours of 05 May (**Figure 6a**). Measurements of the linear depolarization ratio (DPR) reveal that this complex layering structure is comprised of both dust and other pollutants (**Figure 6b**). Large DPR values indicate the presence of non-spherical particles, i.e. dust, with one layer located near the surface, and 3–4 additional layers located between 2 and 8 km AGL ahead of the approaching storm system on 05 May. Layers

corresponding with large backscatter values and low DPR values indicate other pollutants comprised of spherical particles. A cirrus cloud layer arrived ahead of the frontal system at 12.5 km, starting at 00:00 UTC on 05 May. Water clouds attenuated the lidar signal after 08:00 UTC, with a cloud base of ~2 km. Regions where the signal is attenuated are masked in black.

The lowest dust layer arrived in Seoul surmounting the stable nocturnal boundary layer and subsequently mixed to the surface a few hours after sunrise on 04 and 05 May (**Figure 6b**). The presence of these relatively coarse dust particles is confirmed by the corresponding increase in particulate matter with a diameter of less than 10 μm (PM_{10} , **Figure 5c**) observed by the Korean Meteorological Administration (KMA) near the HSRL site in Seoul (KMA station #108, 37.5714°N, 126.9658°E). Elevated levels of surface PM_{10} were also observed during 06–07 May, driven by similar meteorology. The ratio of PM_{10} to $\text{PM}_{2.5}$ (PM ratio) derived from the entire AirKorea network (e.g., **Figure 3**) exceeded 3.0 on 04 May and 07 May (KORUS-AQ average = 1.9), suggesting that dust particles far outnumbered other sources of fine particle pollution near the surface on these dates. Research flights were conducted on all three days, providing detailed measurements of the chemistry and aerosol properties within each individual dust and pollution layer.

Backward trajectories (**Figure 7a**) reveal that all dust and pollution layers highlighted in the 04–05 May HSRL

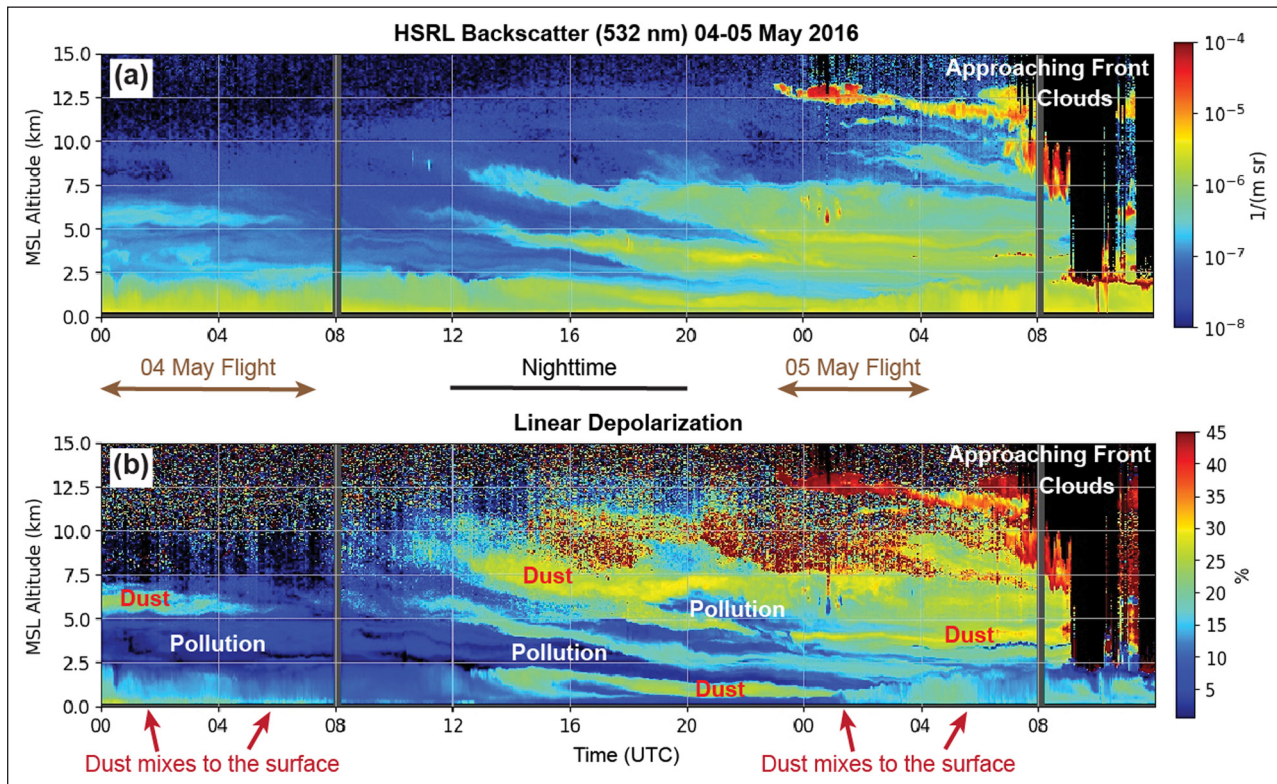


Figure 6: HSRL vertical profiles featuring complex layering of aerosol particles and dust transport. Atmospheric backscatter cross-section at 532 nm (a) and linear depolarization (b) observed by the HSRL in Seoul during a period featuring complex aerosol vertical profiles driven by dynamic meteorology (04–05 May 2016). Altitude is provided above mean sea-level (MSL), which is an approximate AGL altitude (Seoul 38 m MSL). The approximate duration of each NASA DC-8 science flight is denoted by a brown arrow. DOI: <https://doi.org/10.1525/elementa.395.f6>

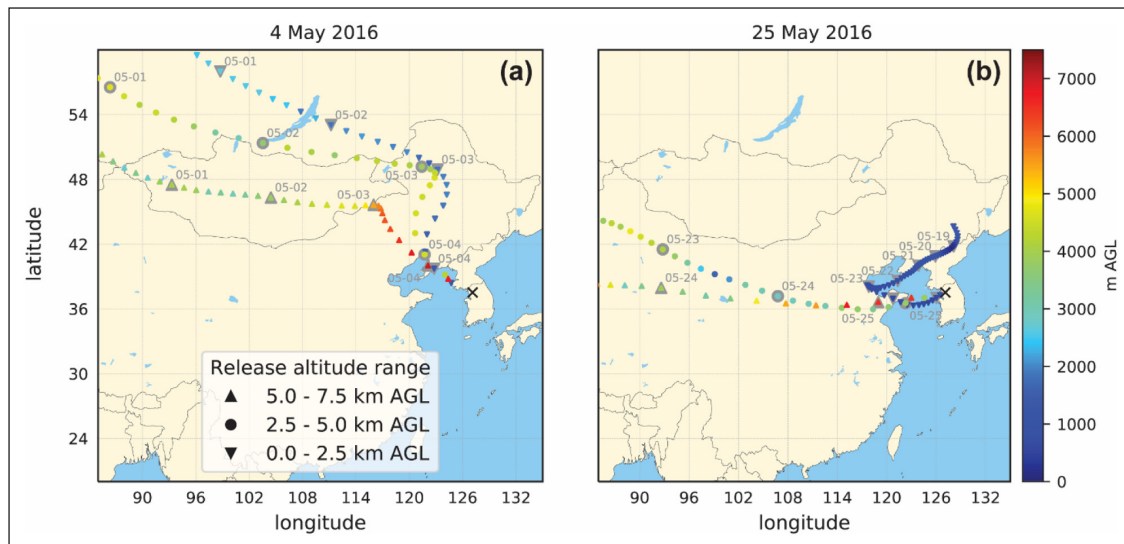


Figure 7: FLEXPART backward trajectories comparing the two dynamic periods of KORUS-AQ. FLEXPART backward trajectories initialized on 04 May 2016 (a) and 25 May 2016 (b). Particles were released in three specific altitude ranges above the Seoul HSRL observation site, coincident with the vertical profiles in Figures 6 and 9. Each trajectory (different symbols for each release altitude range) is plotted at three-hourly time intervals, color coded by its altitude AGL at that time. Points with grey shading and “month-day” annotations indicate positions at 00:00 UTC. DOI: <https://doi.org/10.1525/elementa.395.f7>

display (Figure 6) likely originated near the surface in either northern China or Mongolia over the preceding 3–4 days, and were subsequently lifted by the two mid-latitude cyclones highlighted in Figure 5a–d. These trajectories were calculated with the FLEXible PARTicle (FLEXPART) model (version 10.3; Pissò et al., 2019), driven by six-hourly analyses from the National Centers for Environmental Prediction (NCEP) Global Forecast System (GFS) model (2019), interlaced by the three-hourly forecasts. Using a six hour time window (00:00–06:00 UTC), 250,000 particles were released in three specific altitude ranges above the Seoul HSRL observation site: 0–2.5 km, 2.5–5 km, 5–7.5 km AGL. Particles were followed back in time for one week. Figure 7 displays mass-weighted center trajectories based on the methods of Stohl et al. (2002).

The active storm track driving the complex aerosol vertical profiles observed in early May also produced an environment favorable for stratosphere-to-troposphere exchange from “tropopause folding”, which is often associated with intrusions of stratospheric ozone into the middle and/or upper troposphere (e.g., Hwang et al., 2007). Future studies can employ ozonesonde and aircraft profiles taken during this period of KORUS-AQ for a more detailed examination. The early dynamic period of KORUS-AQ therefore provides an essential dataset for validating the vertical component of chemistry and aerosol transport models, including entrainment of dust particles into the boundary layer, lifting of pollution by strong frontal boundaries, and stratosphere-to-troposphere exchange.

6. Dynamic meteorology, low-level transport, and haze development

The most unhealthy surface air quality observed during KORUS-AQ was related to a series of weak cold fronts, the first of which reached the study region during the even-

ing of 24 May. It traversed the Korean Peninsula from northwest to southeast, and exited the study region by the afternoon of 25 May (Figure 8a). Light southwesterly winds (less than 5 ms^{-1}) were observed within the boundary layer behind the front, facilitating gradual transport of pollution from China into the study region. Modeling results highlight the Shandong Province as the largest contributor during this period (Choi et al., 2019). FLEXPART backward trajectories initialized on 25 May (Figure 7b) confirm the gradual transport of pollution from Shandong Province to Seoul below 2.5 km AGL. A secondary weak cold front on 26 May reinforced this transport pattern, and provided a lifting mechanism for the pollution that arrived in Korea in the wake of the first frontal passage. Conditions remained favorable for transport of Chinese pollution through 27 May.

A second series of two weak cold fronts initiated a separate transport event during 29–31 May, which peaked ahead of the final frontal passage on the morning of 31 May (Figure 8b). In this case, light westerly winds ahead of the approaching front enhanced pollution transport during the morning hours. The front also facilitated convergence and lifting of any pollution that arrived in the study region following the first cold front on 29 May. Northerly winds were observed following the final frontal passage (Figure 8b), effectively ending this transport regime.

Both transport events featured unhealthy levels of ozone (e.g., 60–90 ppbv) and the highest $\text{PM}_{2.5}$ concentrations ($>50 \mu\text{g}/\text{m}^3$) observed at AirKorea ground sites during the campaign (Figure 3). HSRL data highlight the persistent low-level pollution layer observed in Seoul during the first transport event (Figure 9a). Large backscatter values show that the pollution was generally contained within 2 km of the surface, aside from some lifting to 4 km during the secondary frontal passage on

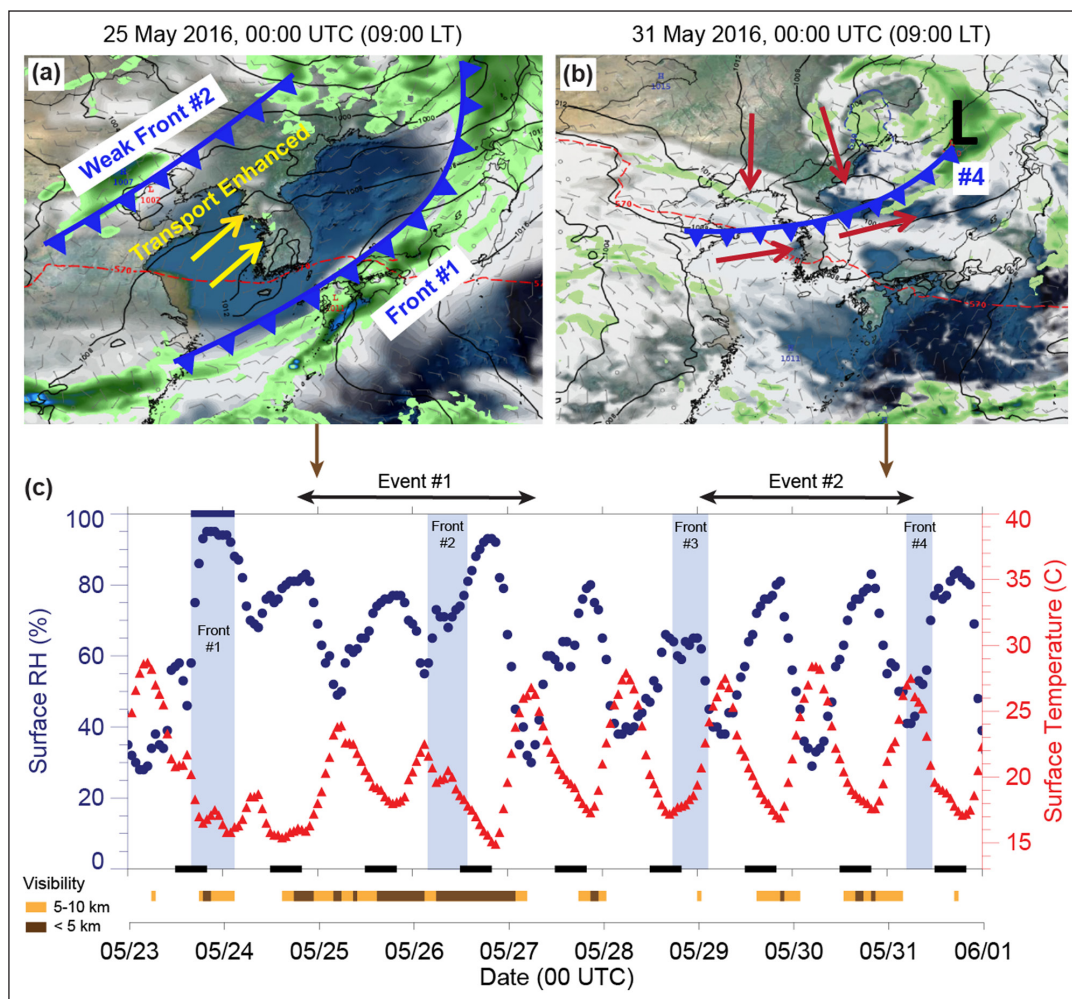


Figure 8: Weaker dynamic forcing, sustained low-level pollution transport, and haze development. Schematics highlighting the synoptic features that initiated the most significant period of low-level pollution transport on 25 May (a) and ended the second period of transport on 31 May (b). Both schematics are based on the 00:00 UTC (09:00 LT) analysis of the Global Air-Land Weather Exploitation Model (GALWEM), with precipitation displayed in green, cloud cover in white, surface wind barbs in gray, and cold fronts in blue. A complete time series of surface temperature (red) and relative humidity (blue) is provided in (c) for an observing station located in Seoul (#108: 37.5714°N, 126.9658°E). Cold front passages are highlighted in light blue, with periods of precipitation indicated by a solid blue bar on the upper x-axis (front #1). Black bars on the bottom x-axis indicate nighttime periods (12:00–20:00 UTC, 21:00–05:00 LT). Periods of reduced surface visibility are displayed in shades of yellow and brown. DOI: <https://doi.org/10.1525/elementa.395.f8>

26 May. This pollution layer coincided with low DPR values, which are indicative of spherical, non-dust aerosols. A few aerosol layers with higher DPR values were observed above the low-level pollution during these transport events (Figure 9b), likely indicating the presence of dust. Backward trajectories initialized at the HSRL site support potential transport of dust particles from northern China above 2.5 km AGL (Figure 7b). However, these layers corresponded with significantly lower backscatter cross-sections than the dynamic period at the beginning of the campaign (Figure 6), and therefore significantly less dust mass. Near-surface fine particle pollution was indeed the primary feature observed during this second period of dynamic meteorology.

Relative humidity (RH) generally remained above 60% near the Olympic Park site in Seoul (Station #108: 37.5714°N, 126.9658°E) from the initial frontal passage

on 24 May until the afternoon of 27 May (Figure 8c). Sustained humid low-level conditions provided an optimal environment for heterogeneous chemical reactions to produce secondary particles, especially during the first and most significant transport event. These included both secondary inorganic aerosols (SIA; e.g., sulfate, nitrate, and ammonium) and secondary organic aerosols (SOA) (Fu and Chen, 2017; Liu et al., 2018). Light surface winds allowed secondary aerosols originating from transboundary pollution to mix with those originating from local sources of pollution. Transboundary pollution (from China) may therefore only partially explain the elevated $PM_{2.5}$ and SOA production observed during this period (e.g., Nault et al., 2018; Jordan et al., manuscript in preparation).

Humid conditions in a shallow boundary layer fostered the production of SIA that in turn promoted the development and persistence of haze (Jordan et al., manuscript in

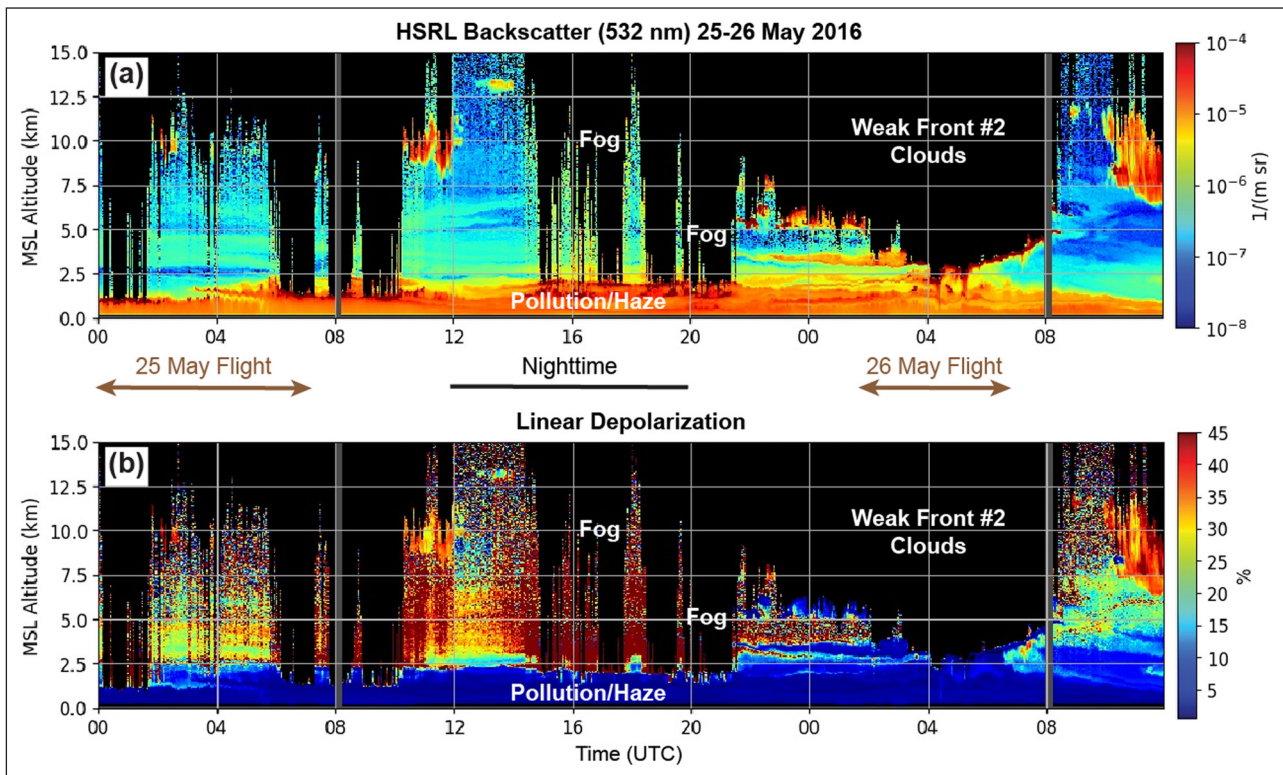


Figure 9: HSRL vertical profiles featuring sustained low-level pollution transport and haze development. Atmospheric backscatter cross-section at 532 nm (a) and linear depolarization (b) observed by the HSRL in Seoul during the most significant period of sustained low-level pollution transport (25–26 May 2016). Altitude is provided above mean sea-level (MSL), which is an approximate AGL altitude (Seoul 38 m MSL). The approximate duration of each NASA DC-8 science flight is denoted by a brown arrow. DOI: <https://doi.org/10.1525/elementa.395.f9>

preparation, and references therein). Gas-phase NO_x (local emissions) and SO_2 (largely from transboundary transport) underwent gas-phase and heterogeneous reactions locally that produced SIA. The hygroscopicity of particulate nitrate and sulfate readily promotes the uptake of water, leading to particle growth that increases available surface area for further SIA production. The positive feedback between SIA production and water uptake provided the essential ingredients for haze development (visibility < 10 km; Tao et al., 2012). **Figure 10a** displays true color satellite imagery from the Visible Infrared Imaging Radiometer Suite (VIIRS) for the afternoon of 25 May. An expansive region of dense haze is evident, extending across the Yellow Sea to the Korean Coastline. Similar conditions persisted through 00:00 UTC on 27 May (09:00 local time [LT]). The study region was essentially located in an extension of the “atmospheric brown cloud” that is often present over eastern China (e.g., Ramanathan et al., 2007).

Observed visibility in Seoul generally remained below 10 km, often falling below 5 km (**Figure 8c**). Vertical profiles of temperature and dew point (radiosonde thermodynamic profiles) obtained at Osan Air Base (RKSO, six-hourly intervals) reveal that this haze event was characterized by a relatively shallow (540–1300 m deep) and moist boundary layer during daytime, surmounted by a significantly drier air mass. An example for 25 May at 06:00 UTC (15:00 LT) is provided in **Figure 10b**. A temperature inversion prevented vertical mixing beyond 1000 m AGL, thus sustaining hazardous pollution levels

near the surface, reinforced by persistent southwesterly transport. The resulting haze layer reduced the solar radiation reaching the surface, which likely contributed to the relatively cool temperatures observed during this event (**Figure 8c**). Over time, this pollution-induced cooling likely reinforced a shallow mixing depth, exemplifying an aerosol-radiation feedback mechanism that has been observed previously in Eastern Asia (e.g., Wang et al., 2014). Shallow mixing depths also support persistent humid conditions (large RH), which support increased secondary particle formation via heterogeneous reactions, further reducing the solar radiation reaching the surface (Liu et al., 2018). These combined feedback loops can rapidly increase fine particle pollution and further reduce visibility at the surface (Wang et al., 2014; Liu et al., 2018).

A shallow, moist boundary layer surmounting relatively cool late spring sea surface temperatures facilitated the development of scattered fog near the Yellow Sea coastline (**Figure 10a**). Foggy conditions were also reported at several stations across Korea, especially near the coast during the nighttime and morning hours of the first transport event. HSRL observations highlight the fog layers observed near Seoul during the first transport event (25–27 May; **Figure 9**). Relatively light surface wind speeds and reduced mixing allowed fog layers to persist. Abundant $\text{PM}_{2.5}$ provided a surplus of available cloud condensation nuclei (CCN), likely resulting in an abundance of small cloud droplets (indirect aerosol effect; Lohmann

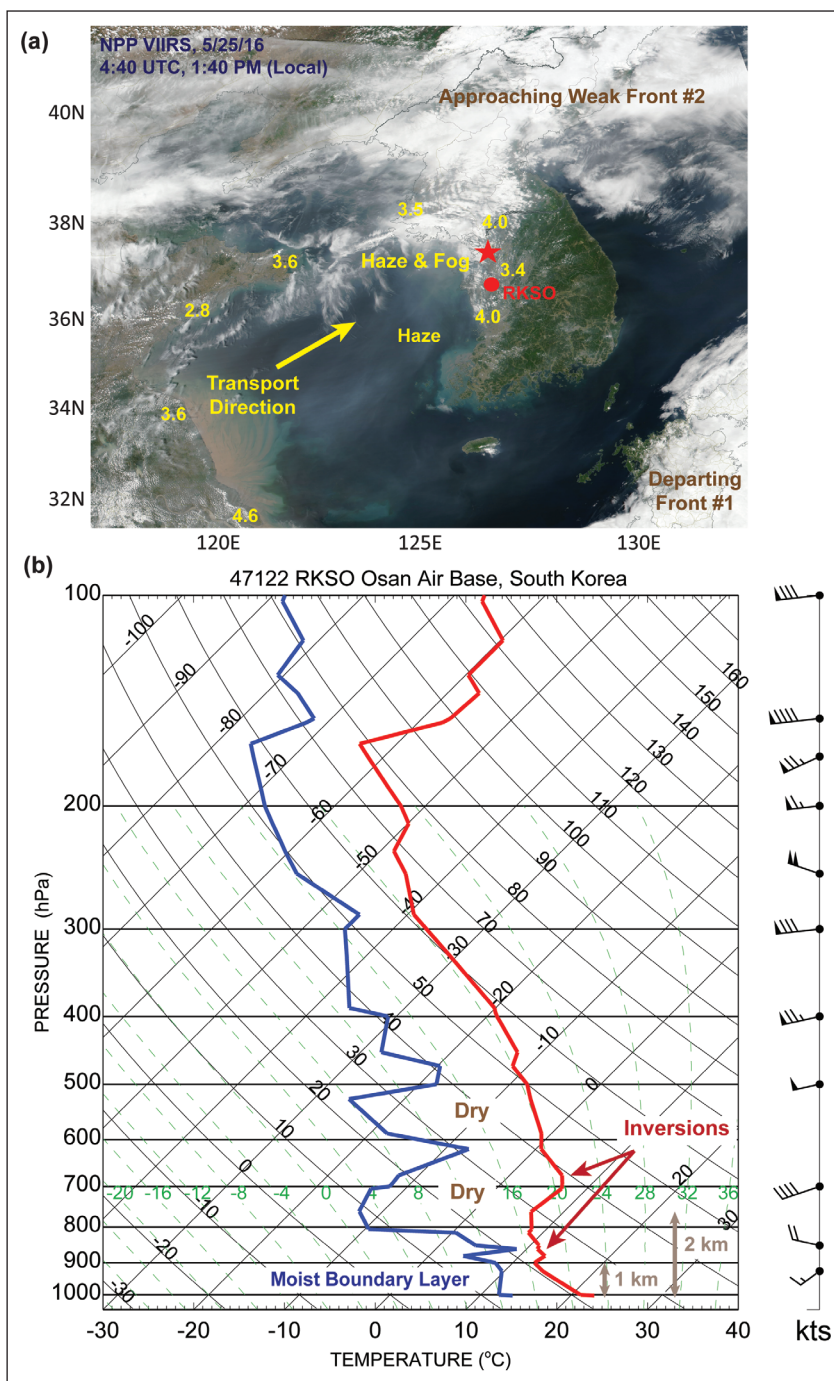


Figure 10: Surface visibility and thermodynamic profile observed during sustained low-level pollution transport. Surface visibility and thermodynamic profile observed during the most significant period of sustained low-level pollution transport during KORUS-AQ. **(a)** VIIRS true color imagery at 04:40 UTC (13:40 LT) on 25 May 2016, with surface visibility observations (km) denoted in yellow. Red star indicates the Seoul Metropolitan Area and red circle indicates the location of Osan Airbase (RKSO). **(b)** Radiosonde profile from RKSO at 06:00 UTC (15:00 LT), with red and blue curves indicating the environmental temperature and dew point, respectively. Profile of wind speed and direction is displayed on the right (1 kt = 0.51 ms⁻¹). DOI: <https://doi.org/10.1525/elementa.395.f10>

and Feichter, 2005). These conditions are known for further enhancing the severity and persistence of fog layers, occasionally resulting in pollution-driven “superfog” (Kokkola et al., 2003; Achtemeier, 2009).

While haze and fog were also observed during the second transport event (29–31 May), observed RH decreased by ~20% during daytime (Figure 8c). Visibility reductions were therefore less severe. Detailed analysis of the

meteorological variables driving these pollution regimes, including the relative strength of frontal boundaries and their inter-annual variability, is essential for understanding unhealthy air quality and poor visibility in Korea, as well as broader regions of eastern Asia. The impact of dense, regional haze events on boundary layer dynamics also remains a significant challenge for numerical weather prediction models.

7. Stagnation under a persistent anticyclone

A significant change in synoptic meteorology occurred during the third week of KORUS-AQ (17–22 May). Stagnant conditions developed in the wake of the final frontal system associated with the early dynamic period. An active jet stream was replaced by a persistent anticyclone and weak synoptic flow (**Figure 4c**). Large-scale subsidence reduced wind speeds and increased surface temperatures, which enhanced ozone production, thereby increasing the total exceedances of Korean air quality standards during daytime (**Figure 3**). However, relatively dry low-level conditions (RH below 40–50%) enhanced nighttime radiative cooling, allowing for relatively low temperatures, and therefore a large diurnal temperature range.

Dry and warm conditions supported daytime mixing depths of 1500–3000 m (via the RKSO, six-hourly

profiles), thus preventing the confinement of $PM_{2.5}$ near the surface. Dry conditions are also unfavorable for abundant secondary aerosol particle formation (Fu and Chen, 2017; Liu et al., 2018), partially explaining the relatively low $PM_{2.5}$ levels observed during this period (**Figure 3**). Another reason stems from the position of the low-level (850 hPa) anticyclone, which induced east-southeasterly winds over much of the study region (**Figure 11a**). This meteorology effectively precluded transport of industrial pollution from other regions of the Asian mainland.

The only exception was potential transport of smoke particles from wildfires in Siberia, which has been observed sporadically during late spring in Korea and Japan (e.g., Lee et al., 2005; Jeong et al., 2008; Ikeda and Tanimoto, 2015). **Figure 11b** displays VIIRS true color imagery and fire detections (750 m) on 18 May (~04:45 UTC, 13:45 LT).

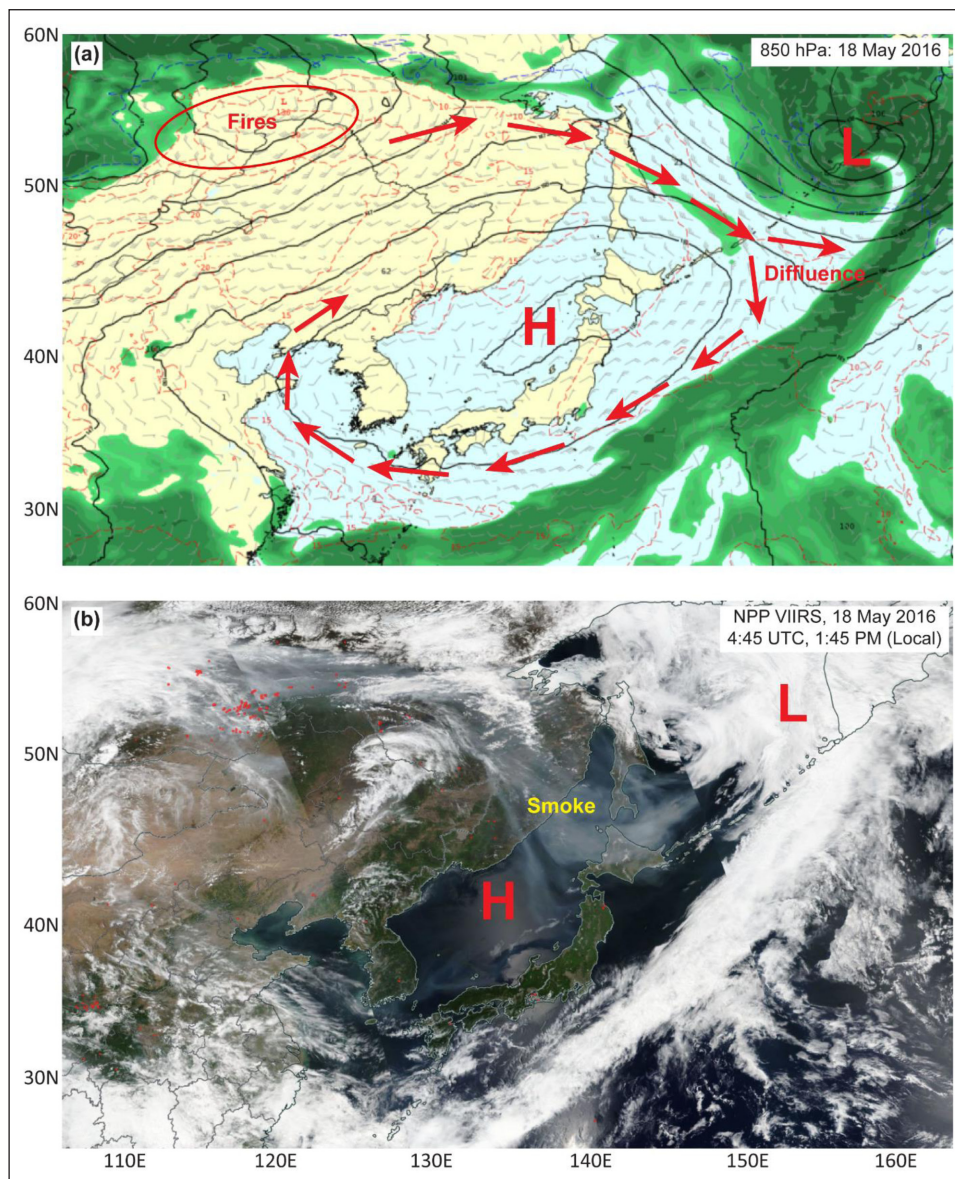


Figure 11: Stagnation under a persistent anticyclone. (a) 850 hPa schematic at the peak of stagnation over Korea. Background image is based on the GALWEM analysis at 18:00 UTC on 18 May 2016, with heights displayed in black, wind barbs in gray, and precipitation in green. Red arrows indicate the general wind pattern. (b) VIIRS true color imagery and fire detections (750 m) at ~04:45 UTC (13:45 LT) on 18 May 2016. DOI: <https://doi.org/10.1525/elementa.395.f11>

A large smoke plume is visible extending from Siberia to northern Japan. This transport is focused along the height gradient between the anticyclone over the study region and a relatively strong mid-latitude cyclone to the northeast of Japan, which was essential for inducing the northerly wind component required for transport of Siberian smoke plumes to the study region. While the majority of the smoke plume continued to move eastward over the Pacific Ocean, a portion of the plume was entrained into the broad anticyclone. This is evidenced by the region of diffluence highlighted in **Figure 11a**. However, when considering the distance traveled and relatively weak low-level wind speeds, any residual smoke particles reaching

the study region were likely significantly aged (e.g., 5–8 days), diffuse, and well mixed with local pollutants.

Minimal impacts from long-distance transport imply that local sources dominated observed pollution levels during this stagnant period. Weak synoptic flow within the anticyclone and stagnant surface conditions enhanced mesoscale and micro-scale meteorological features known to affect local pollution levels. For example, the combination of warm daytime air temperatures (27°C to 30°C) and cool late spring sea surface temperatures (10°C to 15°C) provided an ideal environment for sea breeze development in Korea. **Figure 12** provides a time series of observed RH on 20 May from three ground stations in

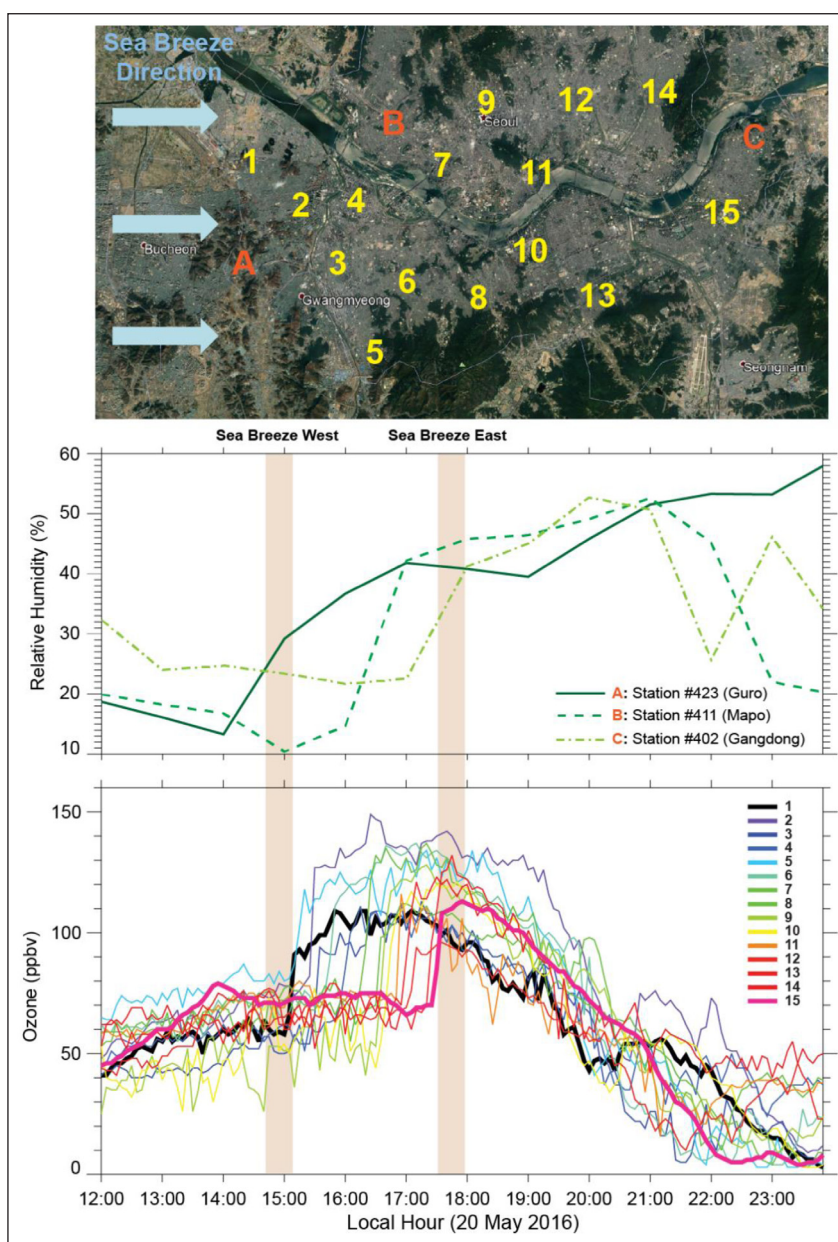


Figure 12: Sea breeze impact on observed ozone levels in Seoul. Sea breeze impact on observed ozone levels in the Seoul Metropolitan Area on the afternoon of 20 May 2016. (Top) Map showing the locations of three weather observing stations (letters) and 15 AirKorea ozone monitoring stations. (Middle) Time series of relative humidity observed at the three weather stations. (Bottom) Time series of ozone levels observed at the 15 AirKorea stations. The approximate arrival and departure of the sea breeze front is highlighted in beige. For reference, downtown Seoul located at 37.57° N, 126.98° E. DOI: <https://doi.org/10.1525/elementa.395.f12>

the Seoul Metropolitan Area, including Guro (423), Mapo (411), and Gangdong (402). The sea breeze is evidenced by a rapid increase in RH associated with the encroaching marine air mass. It crossed the entire region in approximately three hours, arriving at the western station (A) around 15:00 LT, and passing the eastern station (C) near Olympic Park by 18:00 LT.

Ozone observations from 15 AirKorea monitoring sites across the Seoul Metropolitan Area increased by almost 40 ppbv within five minutes as the sea breeze front approached (**Figure 12**, bottom). This rapid change to extremely unhealthy ozone levels (exceeding 120 ppbv) partially resulted from the convergence along the sea breeze front and a subsequent shift to westerly low-level winds, which must traverse the entire Seoul Metropolitan Area before reaching Olympic Park. Persistence of unhealthy ozone levels over Seoul (3–4 hr) is likely a result of transport from a reservoir of ozone production over the Yellow Sea, initiated by the nocturnal land breeze (easterly) transporting ozone precursors off-shore.

Similar variation in ozone levels has been observed under stagnant conditions in many urbanized coastal regions worldwide (e.g., Loughner et al., 2014; Park et al., 2014; Wentworth et al., 2015; Blaylock et al., 2017). Rapid increases in fine particle pollution were also observed in Seoul as the sea breeze traversed the city (Kim et al., 2018). While the sea breeze was the dominant localized weather feature observed during this period, the urban heat island effect, valley/mountain breeze, and river breeze circulations can also affect observed pollution levels in Seoul (e.g., Ryu and Baik, 2013). Understanding the potential impact from these combined circulations on observed air quality remains an important topic for future study.

8. Blocking pattern

The end of the KORUS-AQ measurement period, 01–10 June, was influenced by a blocking pattern over eastern Asia, characterized by a high pressure ridge to the north of an area of lower pressure (**Figure 4d**). This mid-latitude “Rex Block” (Rex, 1950a, b) precluded any significant changes in synoptic meteorology for one week (01–07 June), resulting in occasional stagnant conditions and minimal pollution transport. Local sources dominated observed pollution levels once again. However, conditions at the surface were not as “stagnant” as those observed during the third week of KORUS-AQ.

A strong upper-level jet stream persisted over and to the east of the study region (**Figure 4d**), aligned with the approaching monsoonal boundary (**Figure 2**). Mesoscale disturbances moving along this boundary (driven by deep convection) began to influence local meteorology (Ding and Chan, 2005). Rainfall increased near and to the south of Jeju Island, within the tropical air mass. Interaction between these disturbances and the mid-latitude air mass over the northern portion of the study region induced some variation in surface wind speed, RH, and temperature, affecting pollution levels on a daily basis.

The absence of a persistent pollution regime generally caused $PM_{2.5}$ levels to decrease to within Korean air quality standards, similar to the dynamic period early in the

campaign (**Figure 3**). Ozone levels were likely driven by variation in cloud cover. **Figure 13a** provides a time series of mean daily cloud fraction for the Korean Peninsula derived from AHI (10-min sampling frequency), along with a time series of hourly surface temperature observed in Seoul. While the first two days of the blocking period coincided with relatively few clouds (cloud fraction < 20%), the remaining five days featured cloud fractions above 60% (period mean = 58%). Persistent cloud cover likely suppressed photochemistry, partially explaining the observed reduction in ozone (<60 ppbv) later in the period.

In contrast, the earlier stagnant period (17–22 May) featured unhealthy ozone levels (>60 ppbv) persisting for several days under mostly clear skies and warm temperatures, with minimal variation in meteorology. Periods dominated by stagnation (e.g., persistent anticyclone) and blocking (e.g. Rex Block) can therefore feature distinctive chemistry. The Rex Block decayed by 08 June allowing a final weak cold front to reach the study region. Ozone and $PM_{2.5}$ increased within the post-frontal air mass (**Figure 3**), but not to the extremely unhealthy levels observed during the preceding transport period (25–31 May). A similar blocking pattern developed to the east of the study region during the weeks following KORUS-AQ, affecting the onset and duration of the primary summer rainy season (Changma) over the Korean Peninsula.

9. Contrasting meteorology and observational limitations

As described above, the consecutive stagnant and dynamic transport periods during the middle of KORUS-AQ coincided with the worst surface air quality (**Figure 3**). While both periods featured unhealthy ozone levels (>60 ppbv), $PM_{2.5}$ roughly doubled during the transport events (40–70 $\mu\text{g}/\text{m}^3$ vs. 20–35 $\mu\text{g}/\text{m}^3$), which stand out as the most significant period of fine particle pollution during KORUS-AQ. Observations from these contrasting periods are essential for isolating local emissions and quantifying the contribution of transboundary pollution. However, the contrasting meteorology driving each pollution regime can greatly influence observing conditions.

Figure 13b, c provides a comparison of surface meteorology for both pollution regimes based on anomalies of sea-level pressure (SLP) and surface wind vectors derived from a 30-year climatology (1981–2010; NCEP/NCAR dataset). The stagnant period coincided with positive SLP anomalies exceeding 8.0 mb over the East Sea, where the low-level anticyclone was centered. Positive SLP anomalies were also present over Siberia, indicating a weakened mid-latitude storm track in this region. These combined features supported the observed stagnation over the study region and prevented westerly transport. Conversely, each transport event was characterized by negative SLP anomalies centered to the northeast of the study region, extending inland across central Asia. This feature represents an active mid-latitude storm track, which resulted in the frontal boundaries that ultimately induced westerly pollution transport into the study region.

Large-scale subsidence during the stagnant period facilitated relatively clear and warm conditions (**Figure 13a**),

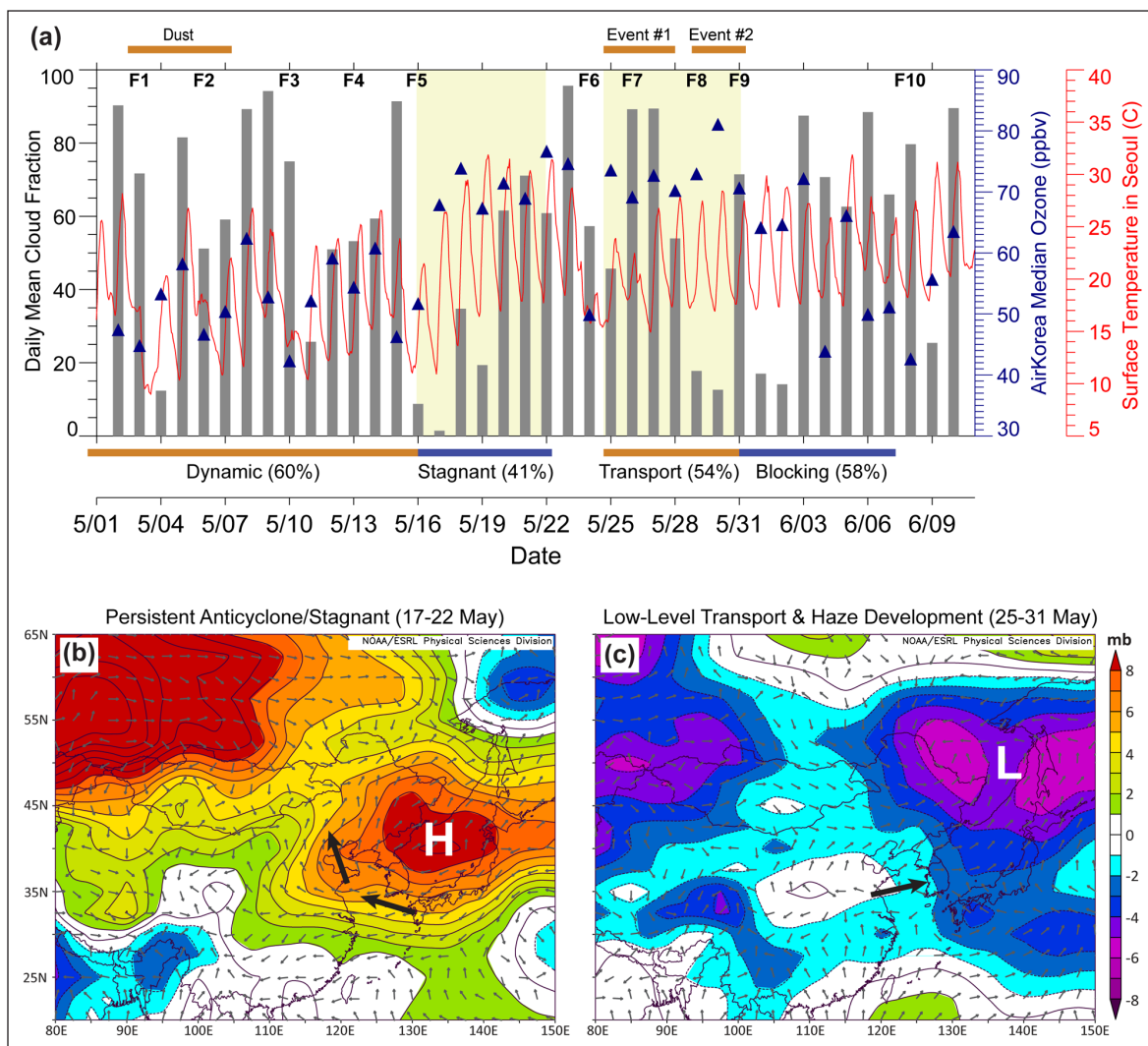


Figure 13: Contrasting meteorology and cloud cover observed during KORUS-AQ. A complete time series of AHI-derived daily cloud fraction (gray bars, 1.0 = completely overcast) and daily median ozone observations (AirKorea, blue triangles) is provided in (a) for the entire Korean Peninsula. Percentages indicate the average cloud fraction observed over the Korean Peninsula during each of the four KORUS-AQ research periods. Red curve indicates hourly surface temperature observed in Seoul (station #108: 37.5714°N, 126.9658°E). Cold front passages are numbered sequentially at the top. Light yellow shading indicates the stagnant and transport periods averaged in (b) and (c), which provide sea-level pressure anomalies derived from the 30-year (1981–2010) NCEP/NCAR climatology (shaded, black contours). Mean surface wind vectors are displayed in black, with bold black arrows indicating the primary pollution transport pattern near Korea. DOI: <https://doi.org/10.1525/elementa.395.f13>

with daily mean cloud fractions below 25% for several days, increasing to 50–60% by the end of the period (mean of 41%). In contrast, the transport periods featured a mean cloud fraction of 54%, with the first and most significant transport event coinciding with cooler temperatures and daily mean cloud fractions between 50% and 90%. The longer period of dynamic meteorology early in the campaign also featured several days with mean cloud fractions above 50% (period mean of 60%).

Enhanced cloudiness presents a significant challenge for remotely sensed observations of air quality parameters that require the presence of sunlight, such as aerosol optical depth (AOD) retrieved from satellite and the ground-based AEROSOL ROBOTIC NETWORK (AERONET; Goddard Space Flight Center, 2019). This observational limitation is primarily driven by the apparent relationship between transport of fine particle pollution and frontal boundaries.

While improved cloud screening techniques have been applied to increase the quantity of valid AOD observations (e.g., Eck et al., 2018), a clear sky bias can still cause a relative underestimation of pollution observed during transport events when compared with stagnant periods dominated by local sources.

10. Representativeness of KORUS-AQ meteorology

Understanding the impact of meteorology on observed pollution during KORUS-AQ requires some perspective on how this period compares to typical late spring conditions. The El Niño/Southern Oscillation (ENSO) and Arctic Oscillation (AO) phenomena are key factors affecting inter-annual climate variability in eastern Asia (e.g., Zang et al., 1997; Park et al., 2011). The strength of the polar jet stream is generally weaker during El Niño, coinciding with

fewer strong cold fronts in Eastern Asia (Zang et al., 1997). Positive AO also generally coincides with relatively weak cold fronts and a westerly wind component (Park et al., 2011). The combination of El Niño and positive AO would therefore favor increased low-level transport of pollution from interior Asia. These conditions would increase the potential for sustained periods of unhealthy surface air quality and poor visibility, similar to those observed during the second period of dynamic meteorology (25–31 May). In contrast, the combination of La Niña and negative AO would support a stronger polar jet stream, stronger cold fronts, and a more northerly low-level wind direction (Park et al., 2011). These conditions favor fewer sustained pollution transport events at the surface, but more potential for airborne dust particles and complex vertical profiles of pollution, similar to those observed during the first dynamic period of KORUS-AQ. The Pacific Decadal Oscillation (PDO) can also impact the meteorology of eastern Asia at longer time scales (e.g., Si et al., 2016). However, diagnosing specific impacts on local pollution regimes is beyond the scope of this study.

While strong El Niño conditions were observed during 2015 and early 2016, a shift to neutral conditions was observed by the start of KORUS-AQ (Climate Prediction Center, 2017). The AO was also near neutral for much of the campaign (Climate Prediction Center, 2005). These climate oscillations therefore had a minimal influence, explaining why observed weather averaged over the entire campaign was very similar to a 30-year climatology (not shown). However, as noted earlier, significant variation was observed within the KORUS-AQ measurement period. The contrasting meteorology driving the stagnant and transport events was the most anomalous (e.g., **Figure 13b, c**), but had an offsetting effect in the full campaign mean.

11. Summary and Conclusions

Hazardous air quality and associated visibility restrictions are highly dependent on variation in meteorology, which in turn drives interactions between trace gases and aerosol particles in the atmosphere. The Korea-United States Air Quality (KORUS-AQ) field study (May–June 2016) provided an unprecedented opportunity to examine the key meteorological conditions driving specific pollution regimes. Meteorology governing the relative influence of local and transboundary pollution sources was explored, including impacts on aerosol vertical structure and surface air quality. This information is essential for interpretation of data collected during KORUS-AQ, as well as development of improved observational tools and forecasting applications.

While the meteorology averaged over the entire campaign generally resembled climatology (30-year dataset), four distinct synoptic patterns were observed within this six-week time period:

1. Dynamic meteorology and complex aerosol vertical profiles (01–16 May);
2. Stagnation under a persistent anticyclone (17–22 May);
3. Dynamic meteorology, low-level transport, and haze development (25–31 May);
4. Blocking pattern (01–07 June).

PM_{2.5} peaked during specific transport events, while unhealthy ozone levels were observed during several periods of contrasting meteorology. Sustained periods of minimal pollution and healthy air quality were absent, regardless of variation in synoptic meteorology. The KORUS-AQ study region therefore remains an important crossroads of pollution in eastern Asia, especially during late spring.

With significant transport of pollution and dust constrained to a few short events, the majority of KORUS-AQ was focused on the impact of local emissions on air quality. During the stagnant period (17–22 May), a persistent anticyclone and weak synoptic flow maximized the influence of Korean emissions. Major sources of local pollution include solvents and mobile sources, such as traffic (Simpson et al., manuscript in preparation). Significant transboundary pollution was blocked, aside from aged smoke from Siberian fires. Stagnation also provided an ideal environment for development of localized circulations. Progression of the sea breeze front across the Seoul Metropolitan Area induced a 40 ppbv increase in ozone concentrations within five minutes. Clear and warm conditions provided an ideal environment for observing enhanced photochemical pollution. However, a clear sky bias likely exists when using satellite data to compare stagnant periods dominated by local pollution with transport events driven by dynamic conditions and associated frontal boundaries.

The two periods of dynamic meteorology were each characterized by an active mid-latitude storm track and a relatively high frequency of cold fronts associated with significant cloud cover. The early period (1–16 May) was the most significant, featuring strong storm systems and frontal boundaries that facilitated sporadic eastward transport of mineral dust and industrial pollution to a broad range of altitudes over the study region. Rapid progression precluded sustained periods of unhealthy surface air quality and reduced visibility.

In contrast, the second dynamic period (25–31 May) featured two sustained transport events, each comprised of three consecutive days with hazardous air quality near the surface. Persistent, low-level transport of general pollution from China was limited to this single period. Weaker frontal boundaries, reduced dynamic forcing, and slower progression allowed pollution to concentrate in a shallow, moist boundary layer, supporting haze/smog development and fog enhancement. Therefore, while frontal boundaries are recognized as the primary mechanism driving pollution transport in eastern Asia (e.g., Liu et al., 2003), only a subset likely facilitate sustained hazardous air quality and reduced visibility at the surface.

Extreme pollution episodes, often featuring poor visibility, remain a common hazard to human health and navigation in Korea and other regions of eastern Asia. Expanding observation networks, modern satellite technology, and improved atmospheric models continue to provide greatly improved inputs for detection, monitoring, and forecasting applications. Quantifying the specific meteorological conditions driving observed pollution regimes is essential for improving these systems. Analysis of the KORUS-AQ springtime period reveals that the key to understanding both the time-averaged pollution

environment in Korea, as well as multi-day forecasts of air quality and visibility, is the convolution of pollution sources and specific meteorology.

Data Accessibility Statement

Regional meteorological plots were generated from the National Center for Environmental Prediction and National Center for Atmospheric Research (NCEP/NCAR) meteorological reanalysis (<https://www.esrl.noaa.gov/psd/data/reanalysis/reanalysis.shtml>). Surface meteorological observations were obtained from the Korea Meteorological Administration (<https://data.kma.go.kr/data/grnd/selectAsosRltmList.do?pgmNo=36>). PM_{2.5} and ozone data were obtained from AirKorea ground monitors (<https://www.airkorea.or.kr/eng>). Lidar displays are based on the High Spectral Resolution Lidar (HSRL) located in Seoul (http://hsrl.ssec.wisc.edu/by_site/). Additional ground and airborne datasets are available from the KORUS-AQ data archive (<https://www-air.larc.nasa.gov/cgi-bin/ArcView/korusaq>).

Acknowledgements

We thank Christopher Camacho (GDIT) and Annette Walker at the Naval Research Laboratory for obtaining and processing surface weather and PM data. We also thank Paolo Veglio at the Space Science and Engineering Center (SSEC, University of Wisconsin-Madison) for providing AH1 cloud fraction data and Sang-Woo Kim at Seoul National University for hosting the HSRL at his laboratory.

Funding information

This project was supported by the NASA KORUS-AQ program under NASA awards NNH16AC52i and NNX-16AD96G. A portion of this research was performed while David Peterson held a Karle's Research Fellowship Award at the Naval Research Laboratory in Monterey, CA. Rokjin Park was supported by the National Research Foundation of Korea (NRF) grant funded by the Korean government (MIST) (No. 2018004494).

Competing interests

The authors have no competing interests to declare.

Author contributions

- Contributed to conception and design: DAP, EJH, JHC, S-OH
- Contributed to acquisition of data: JHC, BLL, RH, REK, EE, CK
- Contributed to analysis and interpretation of data: DAP, EJH, JHC, S-OH, RJP, CK, CEJ
- Drafted and/or revised the article: All authors played a role in drafting/revising the article
- Approved the submitted version for publication: All authors approved the manuscript for publication

References

Achtemeier, GL. 2009. On the formation and persistence of superfog in woodland smoke. *Meteorological Applications* **16**(2): 215–225. DOI: <https://doi.org/10.1002/met.110>

AirKorea. 2018. *AirKorea main webpage*. [online] Available at: <<https://www.airkorea.or.kr/eng>> [accessed 08 October 2019].

Bey, I, Jacob, DJ, Logan, JA and Yantosca, RM. 2001. Asian chemical outflow to the Pacific in spring: Origins, pathways, and budgets. *Journal of Geophysical Research-Atmospheres* **106**(D19): 23097–23113. DOI: <https://doi.org/10.1029/2001JD000806>

Blaylock, BK, Horel, JD and Crosman, ET. 2017. Impact of Lake Breezes on Summer Ozone Concentrations in the Salt Lake Valley. *Journal of Applied Meteorology and Climatology* **56**(2): 353–370. DOI: <https://doi.org/10.1175/JAMC-D-16-0216.1>

Chen, SJ, Kuo, YH, Zhang, PZ and Bai, QF. 1991. Synoptic climatology of cyclogenesis over East-Asia, 1958–1987. *Monthly Weather Review* **119**(6): 1407–1418. DOI: [https://doi.org/10.1175/1520-0493\(1991\)119<1407:SCOCOE>2.0.CO;2](https://doi.org/10.1175/1520-0493(1991)119<1407:SCOCOE>2.0.CO;2)

Chen, SY, Huang, JP, Kang, LT, Wang, H, Ma, XJ, He, YL, Yuan, TG, Yang, B, Huang, ZW and Zhang, GL. 2017. Emission, transport, and radiative effects of mineral dust from the Taklimakan and Gobi deserts: comparison of measurements and model results. *Atmospheric Chemistry and Physics* **17**(3): 2401–2421. DOI: <https://doi.org/10.5194/acp-17-2401-2017>

Choi, J, Park, RJ, Lee, HM, Lee, S, Jo, DS, Jeong, JI, Henze, DK, Woo, JH, Ban, SJ, Lee, MD, Lim, CS, Park, MK, Shin, HJ, Cho, S, Peterson, D and Song, CK. 2019. Impacts of local vs. trans-boundary emissions from different sectors on PM_{2.5} exposure in South Korea during the KORUS-AQ campaign. *Atmospheric Environment* **203**: 196–205. DOI: <https://doi.org/10.1016/j.atmosenv.2019.02.008>

Choi, M, Kim, J, Lee, J, Kim, M, Park, YJ, Holben, B, Eck, TF, Li, ZQ and Song, CH. 2018. GOCI Yonsei aerosol retrieval version 2 products: An improved algorithm and error analysis with uncertainty estimation from 5-year validation over East Asia. *Atmospheric Measurement Techniques* **11**(1): 385–408. DOI: <https://doi.org/10.5194/amt-11-385-2018>

Climate Prediction Center. 2005. *Arctic Oscillation (AO)*. [online] Available at: <https://www.cpc.ncep.noaa.gov/products/precip/CWlink/daily_ao_index/ao.shtml> [accessed 08 October 2019].

Climate Prediction Center. 2017. *Monthly Niño-3.4 Index*. [online] Available at: <https://origin.cpc.ncep.noaa.gov/products/analysis_monitoring/ensostuff/ONI_change.shtml> [accessed 08 October 2019].

Crawford, JH. Manuscript in preparation. Overview of KORUS-AQ. *Elementa* (this issue).

Demuzere, M, Trigo, RM, de Arellano, JVG and van Lipzig, NPM. 2009. The impact of weather and atmospheric circulation on O₃ and PM₁₀ levels at a rural mid-latitude site. *Atmospheric Chemistry and Physics* **9**(8): 2695–2714. DOI: <https://doi.org/10.5194/acp-9-2695-2009>

- Ding, YH and Chan, JCL.** 2005. The East Asian summer monsoon: An overview. *Meteorology and Atmospheric Physics* **89**(1–4): 117–142. DOI: <https://doi.org/10.1007/s00703-005-0125-z>
- Eck, TF, Holben, BN, Reid, JS, Xian, P, Giles, DM, Sinyuk, A, Smirnov, A, Schafer, JS, Slutsker, I, Kim, J, Koo, JH, Choi, M, Kim, KC, Sano, I, Arola, A, Sayer, AM, Levy, RC, Munchak, LA, O'Neill, NT, Lyapustin, A, Hsu, NC, Randles, CA, Da Silva, AM, Buchard, V, Govindaraju, RC, Hyer, E, Crawford, JH, Wang, P and Xia, X.** 2018. Observations of the Interaction and Transport of Fine Mode Aerosols With Cloud and/or Fog in Northeast Asia From Aerosol Robotic Network and Satellite Remote Sensing. *Journal of Geophysical Research-Atmospheres* **123**(10): 5560–5587. DOI: <https://doi.org/10.1029/2018JD028313>
- Eckhardt, S, Stohl, A, Wernli, H, James, P, Forster, C and Spichtinger, N.** 2004. A 15-year climatology of warm conveyor belts. *Journal of Climate* **17**(1): 218–237. DOI: [https://doi.org/10.1175/1520-0442\(2004\)017<0218:AYCOWC>2.0.CO;2](https://doi.org/10.1175/1520-0442(2004)017<0218:AYCOWC>2.0.CO;2)
- Flowers, BA, Dubey, MK, Mazzoleni, C, Stone, EA, Schauer, JJ, Kim, SW and Yoon, SC.** 2010. Optical-chemical-microphysical relationships and closure studies for mixed carbonaceous aerosols observed at Jeju Island; 3-laser photoacoustic spectrometer, particle sizing, and filter analysis. *Atmospheric Chemistry and Physics* **10**(21): 10387–10398. DOI: <https://doi.org/10.5194/acp-10-10387-2010>
- Fromm, M, Kablick, G and Caffrey, P.** 2016. Dust-infused baroclinic cyclone storm clouds: The evidence, meteorology, and some implications. *Geophysical Research Letters* **43**(24): 12643–12650. DOI: <https://doi.org/10.1002/2016GL071801>
- Fu, HB and Chen, JM.** 2017. Formation, features and controlling strategies of severe haze-fog pollutions in China. *Science of the Total Environment* **578**: 121–138. DOI: <https://doi.org/10.1016/j.scitotenv.2016.10.201>
- Fuelberg, HE, Kiley, CM, Hannan, JR, Westberg, DJ, Avery, MA and Newell, RE.** 2003. Meteorological conditions and transport pathways during the Transport and Chemical Evolution over the Pacific (TRACE-P) experiment. *Journal of Geophysical Research-Atmospheres* **108**(D20). DOI: <https://doi.org/10.1029/2002JD003092>
- GEO-CAPE.** 2015. *Advancing the science of both coastal ocean biophysics and atmospheric pollution chemistry: A White Paper report to the NASA Earth Science Division by the GEO-CAPE Team.* [online] Available at: https://geo-cape.larc.nasa.gov/pdf/GEO-CAPE_2009-2015_SummativeWhitePaper.pdf [accessed 08 October 2019].
- Goddard Space Flight Center.** 2019. *Aerosol Robotic Network.* [online] Available at: <https://aeronet.gsfc.nasa.gov/> [accessed 08 October 2019].
- Ha, R, Baatar, A and Yu, Y.** 2017. Identification of atmospheric transport and dispersion of Asian dust storms. *Natural Hazards and Earth System Sciences* **17**(8): 1425–1435. DOI: <https://doi.org/10.5194/nhess-17-1425-2017>
- Holben, BN, Tanre, D, Smirnov, A, Eck, TF, Slutsker, I, Abuhassan, N, Newcomb, WW, Schafer, JS, Chatenet, B, Lavenu, F, Kaufman, YJ, Castle, JV, Setzer, A, Markham, B, Clark, D, Frouin, R, Halthore, R, Karneli, A, O'Neill, NT, Pietras, C, Pinker, RT, Voss, K and Zibordi, G.** 2001. An emerging ground-based aerosol climatology: Aerosol optical depth from AERONET. *Journal of Geophysical Research-Atmospheres* **106**(D11): 12067–12097. DOI: <https://doi.org/10.1029/2001JD900014>
- Huang, K, Zhuang, G, Lin, Y, Fu, JS, Wang, Q, Liu, T, Zhang, R, Jiang, Y, Deng, C, Fu, Q, Hsu, NC and Cao, B.** 2012. Typical types and formation mechanisms of haze in an Eastern Asia megacity, Shanghai. *Atmospheric Chemistry and Physics* **12**(1): 105–124. DOI: <https://doi.org/10.5194/acp-12-105-2012>
- Hwang, SH, Kim, J and Cho, GR.** 2007. Observation of secondary ozone peaks near the tropopause over the Korean peninsula associated with stratosphere-troposphere exchange. *Journal of Geophysical Research-Atmospheres* **112**(D16). DOI: <https://doi.org/10.1029/2006JD007978>
- Ikedo, K and Tanimoto, H.** 2015. Exceedances of air quality standard level of PM_{2.5} in Japan caused by Siberian wildfires. *Environmental Research Letters* **10**(10). DOI: <https://doi.org/10.1088/1748-9326/10/10/105001>
- Itahashi, S, Uno, I and Kim, S.** 2013. Seasonal source contributions of tropospheric ozone over East Asia based on CMAQ-HDDM. *Atmospheric Environment* **70**: 204–217. DOI: <https://doi.org/10.1016/j.atmosenv.2013.01.026>
- Itahashi, S, Yumimoto, K, Uno, I, Eguchi, K, Takemura, T, Hara, Y, Shimizu, A, Sugimoto, N and Liu, ZY.** 2010. Structure of dust and air pollutant outflow over East Asia in the spring. *Geophysical Research Letters* **37**. DOI: <https://doi.org/10.1029/2010GL044776>
- Jacob, DJ, Crawford, JH, Kleb, MM, Connors, VS, Bendura, RJ, Raper, JL, Sachse, GW, Gille, JC, Emmons, L and Heald, CL.** 2003. Transport and Chemical Evolution over the Pacific (TRACE-P) aircraft mission: Design, execution, and first results. *Journal of Geophysical Research-Atmospheres* **108**(D20): 1–19. DOI: <https://doi.org/10.1029/2002JD003276>
- Jeong, JI, Park, RJ and Yeh, SW.** 2018. Dissimilar effects of two El Nino types on PM_{2.5} concentrations in East Asia. *Environmental Pollution* **242**: 1395–1403. DOI: <https://doi.org/10.1016/j.envpol.2018.08.031>
- Jeong, JI, Park, RJ and Youn, D.** 2008. Effects of Siberian forest fires on air quality in East Asia during May 2003 and its climate implication. *Atmospheric Environment* **42**(39): 8910–8922. DOI: <https://doi.org/10.1016/j.atmosenv.2008.08.037>
- Jordan, CE, Crawford, JH, Beyersdorf, AJ, Eck, TF, Halliday, HS, Nault, BA, Chang, L-S, Park, R, Lee, G, Kim, H, Cho, S, Shin, HJ, Lee, JH, Jung, J, Kim, D-S, Lee, M, Lee, T, Whitehill, A, Szykman, J,**

- Schueneman, MK, Jost, PC, Jimenez, JL, DiGangi, JP, Diskin, GS, Anderson, BE, Moore, RH, Ziemba, LD, Fenn, MA, Hair, JW, Kuehn, RE, Holz, RE, Chen, G, Travis, K, Shook, M, Peterson, DA, Lamb, KD and Schwarz, JP.** manuscript in preparation. Investigation of factors controlling PM_{2.5} variability across the South Korean peninsula during KORUS-AQ. *Elementa* (this issue).
- Jung, MI, Son, SW, Kim, HC, Kim, SW, Park, RJ and Chen, D.** 2019. Contrasting synoptic weather patterns between non-dust high particulate matter events and Asian dust events in Seoul, South Korea. *Atmospheric Environment* **214**. DOI: <https://doi.org/10.1016/j.atmosenv.2019.116864>
- Kampa, M and Castanas, E.** 2008. Human health effects of air pollution. *Environmental Pollution* **151**(2): 362–367. DOI: <https://doi.org/10.1016/j.envpol.2007.06.012>
- Kim, H and Chung, Y.** 2005. On surface O₃ associated with long-range transport in the Yellow Sea region. *Water Air and Soil Pollution* **165**(1–4): 95–112. DOI: <https://doi.org/10.1007/s11270-005-4639-2>
- Kim, H, Zhang, Q and Heo, J.** 2018. Influence of intense secondary aerosol formation and long-range transport on aerosol chemistry and properties in the Seoul Metropolitan Area during spring time: Results from KORUS-AQ. *Atmospheric Chemistry and Physics* **18**(10): 7149–7168. DOI: <https://doi.org/10.5194/acp-18-7149-2018>
- Kim, Y, Kim, SW, Yoon, SC, Kim, MH and Park, KH.** 2014. Aerosol properties and associated regional meteorology during winter pollution event at Gosan climate observatory, Korea. *Atmospheric Environment* **85**: 9–17. DOI: <https://doi.org/10.1016/j.atmosenv.2013.11.041>
- Kokkola, H, Romakkaniemi, S and Laaksonen, A.** 2003. On the formation of radiation fogs under heavily polluted conditions. *Atmospheric Chemistry and Physics* **3**: 581–589. DOI: <https://doi.org/10.5194/acp-3-581-2003>
- Lamb, KD, Perring, AE, Samset, B, Peterson, D, Davis, S, Anderson, BE, Beyersdorf, A, Blake, DR, Campuzano-Jost, P, Corr, CA, Diskin, GS, Kondo, Y, Moteki, N, Nault, BA, Oh, J, Park, M, Pusede, SE, Simpson, IJ, Thornhill, KL, Wisthaler, A and Schwarz, JP.** 2018. Estimating Source Region Influences on Black Carbon Abundance, Microphysics, and Radiative Effect Observed Over South Korea. *Journal of Geophysical Research-Atmospheres* **123**(23): 13527–13548. DOI: <https://doi.org/10.1029/2018JD029257>
- Lee, JY, Kwon, M, Yun, KS, Min, SK, Park, IH, Ham, YG, Jin, EK, Kim, JH, Seo, KH, Kim, W, Yim, SY and Yoon, JH.** 2017. The long-term variability of Changma in the East Asian summer monsoon system: A review and revisit. *Asia-Pacific Journal of Atmospheric Sciences* **53**(2): 257–272. DOI: <https://doi.org/10.1007/s13143-017-0032-5>
- Lee, KH, Kim, JE, Kim, YJ, Kim, J and von Hoyningen-Huene, W.** 2005. Impact of the smoke aerosol from Russian forest fires on the atmospheric environment over Korea during May 2003. *Atmospheric Environment* **39**(1): 85–99. DOI: <https://doi.org/10.1016/j.atmosenv.2004.09.032>
- Lee, YG, Ho, CH, Kim, JH and Kim, J.** 2015. Quiescence of Asian dust events in South Korea and Japan during 2012 spring: Dust outbreaks and transports. *Atmospheric Environment* **114**: 92–101. DOI: <https://doi.org/10.1016/j.atmosenv.2015.05.035>
- Lennartson, EM, Wang, J, Gu, JP, Garcia, LC, Ge, C, Gao, M, Choi, M, Saide, PE, Carmichael, GR, Kim, J and Janz, SJ.** 2018. Diurnal variation of aerosol optical depth and PM_{2.5} in South Korea: a synthesis from AERONET, satellite (GOCI), KORUS-AQ observation, and the WRF-Chem model. *Atmospheric Chemistry and Physics* **18**(20): 15125–15144. DOI: <https://doi.org/10.5194/acp-18-15125-2018>
- Liao, ZH, Gao, M, Sun, JR and Fan, SJ.** 2017. The impact of synoptic circulation on air quality and pollution-related human health in the Yangtze River Delta region. *Science of the Total Environment* **607**: 838–846. DOI: <https://doi.org/10.1016/j.scitotenv.2017.07.031>
- Liu, CM, Buhr, M and Merrill, JT.** 1997. Ground-based observation of ozone, carbon monoxide, and sulfur dioxide at Kenting, Taiwan, during the PEM-West B campaign. *Journal of Geophysical Research-Atmospheres* **102**(D23): 28613–28625. DOI: <https://doi.org/10.1029/96JD02980>
- Liu, HY, Jacob, DJ, Bey, I, Yantosca, RM, Duncan, BN and Sachse, GW.** 2003. Transport pathways for Asian pollution outflow over the Pacific: Interannual and seasonal variations. *Journal of Geophysical Research-Atmospheres* **108**(D20). DOI: <https://doi.org/10.1029/2002JD003102>
- Liu, JJ, Zheng, YF, Li, ZQ, Flynn, C, Welton, EJ and Cribb, M.** 2011. Transport, vertical structure and radiative properties of dust events in southeast China determined from ground and space sensors. *Atmospheric Environment* **45**(35): 6469–6480. DOI: <https://doi.org/10.1016/j.atmosenv.2011.04.031>
- Liu, Q, Jia, X, Quan, J, Li, J, Li, X, Wu, Y, Chen, D, Wang, Z and Liu, Y.** 2018. New positive feedback mechanism between boundary layer meteorology and secondary aerosol formation during severe haze events. *Scientific Reports* **8**. DOI: <https://doi.org/10.1038/s41598-018-24366-3>
- Liu, X, Zhang, Y, Jung, J, Gu, J, Li, Y, Guo, S, Chang, S-Y, Yue, D, Lin, P, Kim, YJ, Hu, M, Zeng, L and Zhu, T.** 2009. Research on the hygroscopic properties of aerosols by measurement and modeling during CAREBeijing-2006. *Journal of Geophysical Research-Atmospheres* **114**. DOI: <https://doi.org/10.1029/2008JD010805>
- Liu, Y, Yang, D, Chen, W and Zhang, H.** 2010. Measurements of Asian dust optical properties over the Yellow Sea of China by shipboard and ground-based photometers, along with satellite remote sensing: A case study of the passage of a frontal system during April 2006. *Journal of Geophysical*

- Research-Atmospheres* **115**. DOI: <https://doi.org/10.1029/2009JD012684>
- Liu, YK, Liu, JF and Tao, S.** 2013. Interannual variability of summertime aerosol optical depth over East Asia during 2000-2011: a potential influence from El Nino Southern Oscillation. *Environmental Research Letters* **8**(4). DOI: <https://doi.org/10.1088/1748-9326/8/4/044034>
- Lohmann, U and Feichter, J.** 2005. Global indirect aerosol effects: A review. *Atmospheric Chemistry and Physics* **5**: 715–737. DOI: <https://doi.org/10.5194/acp-5-715-2005>
- Loughner, CP, Tzortziou, M, Follette-Cook, M, Pickering, KE, Goldberg, D, Satam, C, Weinheimer, A, Crawford, JH, Knapp, DJ, Montzka, DD, Diskin, GS and Dickerson, RR.** 2014. Impact of Bay-Breeze Circulations on Surface Air Quality and Boundary Layer Export. *Journal of Applied Meteorology and Climatology* **53**(7): 1697–1713. DOI: <https://doi.org/10.1175/JAMC-D-13-0323.1>
- National Centers for Environmental Prediction/National Weather Service/NOAA/U.S. Department of Commerce, Research Data Archive at the National Center for Atmospheric Research, Computational and Information Systems Laboratory, Boulder, CO, updated daily. *NCEP FNL Operational Model Global Tropospheric Analyses, continuing from July 1999*. [online] [accessed 01 October 2019]. DOI: <https://doi.org/10.5065/D6M043C6>
- Nault, BA, Campuzano-Jost, P, Day, DA, Schroder, JC, Anderson, B, Beyersdorf, AJ, Blake, DR, Brune, WH, Choi, Y, Corr, CA, de Gouw, JA, Dibb, J, DiGangi, JP, Diskin, GS, Fried, A, Huey, LG, Kim, MJ, Knute, CJ, Lamb, KD, Lee, T, Park, T, Pusede, SE, Scheuer, E, Thornhill, KL, Woo, J-H and Jimenez, JL.** 2018. Secondary organic aerosol production from local emissions dominates the organic aerosol budget over Seoul, South Korea, during KORUS-AQ. *Atmospheric Chemistry and Physics* **18**(24): 17769–17800. DOI: <https://doi.org/10.5194/acp-18-17769-2018>
- Oltmans, SJ, Johnson, BJ, Harris, JM, Thompson, AM, Liu, HY, Chan, CY, Vomel, H, Fujimoto, T, Brackett, VG, Chang, WL, Chen, JP, Kim, JH, Chan, LY and Chang, HW.** 2004. Tropospheric ozone over the North Pacific from ozonesonde observations. *Journal of Geophysical Research-Atmospheres* **109**(D15). DOI: <https://doi.org/10.1029/2003JD003466>
- Park, S-Y, Lee, S-H and Lee, HW.** 2014. Assimilation of wind profiler observations and its impact on three-dimensional transport of ozone over the Southeast Korean Peninsula. *Atmospheric Environment* **99**: 660–672. DOI: <https://doi.org/10.1016/j.atmosenv.2014.09.082>
- Park, T-W, Ho, C-H and Yang, S.** 2011. Relationship between the Arctic Oscillation and Cold Surges over East Asia. *Journal of Climate* **24**(1): 68–83. DOI: <https://doi.org/10.1175/2010JCLI3529.1>
- Pisso, I, Sollum, E, Grythe, H, Kristiansen, NI, Cassiani, M, Eckhardt, S, Arnold, D, Morton, D, Thompson, RL, Zwaafink, CDG, Evangeliou, N, Sodemann, H, Haimberger, L, Henne, S, Brunner, D, Burkhardt, JF, Fouilloux, A, Brioude, J, Philipp, A, Seibert, P and Stohl, A** in review. The Lagrangian particle dispersion model FLEXPART version 10.3. *Geoscientific Model Development Discussions*. [online] Available at: <https://www.geoscientific-model-dev-discuss.net/gmd-2018-333/> [accessed 15 October 2019]. DOI: <https://doi.org/10.5194/gmd-2018-333>
- Ramanathan, V, Li, F, Ramana, MV, Praveen, PS, Kim, D, Corrigan, CE, Nguyen, H, Stone, EA, Schauer, JJ, Carmichael, GR, Adhikary, B and Yoon, SC.** 2007. Atmospheric brown clouds: Hemispherical and regional variations in long-range transport, absorption, and radiative forcing. *Journal of Geophysical Research-Atmospheres* **112**(D22). DOI: <https://doi.org/10.1029/2006JD008124>
- Ren, YQ, Wang, GH, Li, JJ, Wu, C, Cao, C, Li, J, Wang, JY, Ge, SS, Xie, YN, Li, XR, Meng, F and Li, H.** 2019. Evolution of aerosol chemistry in Xi'an during the spring dust storm periods: Implications for heterogeneous formation of secondary organic aerosols on the dust surface. *Chemosphere* **215**: 413–421. DOI: <https://doi.org/10.1016/j.chemosphere.2018.10.064>
- Rex, DF.** 1950a. Blocking Action in the Middle Troposphere and its Effect upon Regional Climate I. An Aerological Study of Blocking Action. *Tellus* **2**(3): 196–211. DOI: <https://doi.org/10.3402/tellusa.v2i3.8546>
- Rex, DF.** 1950b. Blocking Action in the Middle Troposphere and its Effect upon Regional Climate II. The Climatology of Blocking Action. *Tellus* **2**(4): 275–301. DOI: <https://doi.org/10.3402/tellusa.v2i4.8603>
- Ryu, YH and Baik, JJ.** 2013. Daytime Local Circulations and Their Interactions in the Seoul Metropolitan Area. *Journal of Applied Meteorology and Climatology* **52**(4): 784–801. DOI: <https://doi.org/10.1175/JAMC-D-12-0157.1>
- Sampe, T and Xie, SP.** 2010. Large-Scale Dynamics of the Meiyu-Baiu Rainband: Environmental Forcing by the Westerly Jet. *Journal of Climate* **23**(1): 113–134. DOI: <https://doi.org/10.1175/2009JCLI3128.1>
- Shang, Y, Sun, Z, Cao, J, Wang, X, Zhong, L, Bi, X, Li, H, Liu, W, Zhu, T and Huang, W.** 2013. Systematic review of Chinese studies of short-term exposure to air pollution and daily mortality. *Environment International* **54**: 100–111. DOI: <https://doi.org/10.1016/j.envint.2013.01.010>
- Shao, Y and Dong, CH.** 2006. A review on East Asian dust storm climate, modelling and monitoring. *Global and Planetary Change* **52**(1–4): 1–22. DOI: <https://doi.org/10.1016/j.gloplacha.2006.02.011>
- Shin, SK, Mueller, D, Lee, C, Lee, KH, Shin, D, Kim, YJ and Noh, YM.** 2015. Vertical variation of optical properties of mixed Asian dust/pollution plumes according to pathway of air mass transport over East Asia. *Atmospheric Chemistry and Physics* **15**(12): 6707–6720. DOI: <https://doi.org/10.5194/acp-15-6707-2015>

- Si, D** and **Ding, YH**. 2016. Oceanic Forcings of the Interdecadal Variability in East Asian Summer Rainfall. *Journal of Climate* **29**(21): 7633–7649. DOI: <https://doi.org/10.1175/JCLI-D-15-0792.1>
- Simpson, IJ, Blake, DR, Blake, NJ, Meinardi, S, Barletta, B, Hughes, SC, Fleming, LT, Crawford, JH, Diskin, GS, Emmons, LK, Fried, A, Guo, H, Peterson, DA, Wisthaler, A, Woo, J-H, Barré, J, Gaubert, B, Kim, J, Kim, MJ, Kim, Y, Knote, C, Mikoviny, T, Pusede, SE, Schroeder, JR, Wang, Y, Wennberg, PO and Zeng, L**. manuscript in preparation. Characterization, sources and reactivity of volatile organic compounds (VOCs) in Seoul and surrounding regions during KORUS-AQ. *Elementa* (this issue).
- Stohl, A, Eckhardt, S, Forster, C, James, P, Spichtinger, N and Seibert, P**. 2002. A replacement for simple back trajectory calculations in the interpretation of atmospheric trace substance measurements. *Atmospheric Environment* **36**(29): 4635–4648. DOI: [https://doi.org/10.1016/S1352-2310\(02\)00416-8](https://doi.org/10.1016/S1352-2310(02)00416-8)
- Takemi, T and Seino, N**. 2005. Dust storms and cyclone tracks over the arid regions in east Asia in spring. *Journal of Geophysical Research-Atmospheres* **110**(D18). DOI: <https://doi.org/10.1029/2004JD004698>
- Tao, MH, Chen, LF, Su, L and Tao, JH**. 2012. Satellite observation of regional haze pollution over the North China Plain. *Journal of Geophysical Research-Atmospheres* **117**. DOI: <https://doi.org/10.1029/2012JD017915>
- Tsay, SC, Maring, HB, Lin, NH, Buntoung, S, Chantara, S, Chuang, HC, Gabriel, PM, Goodloe, CS, Holben, BN, Hsiao, TC, Hsu, NC, Janjai, S, Lau, WKM, Lee, CT, Lee, J, Loftus, AM, Nguyen, AX, Nguyen, CM, Pani, SK, Pantina, P, Sayer, AM, Tao, WK, Wang, SH, Welton, EJ, Wiriya, W and Yen, MC**. 2016. Satellite-Surface Perspectives of Air Quality and Aerosol-Cloud Effects on the Environment: An Overview of 7-SEAS/BASELInE. *Aerosol and Air Quality Research* **16**(11): 2581–2602. DOI: <https://doi.org/10.4209/aaqr.2016.08.0350>
- University of Wisconsin**. 2019. *University of Wisconsin – Madison HSRL Data Archives*. [online] Available at: http://hsrl.ssec.wisc.edu/by_site/ [accessed 08 October 2019].
- Wang, JD, Wang, SX, Jiang, JK, Ding, AJ, Zheng, M, Zhao, B, Wong, DC, Zhou, W, Zheng, GJ, Wang, L, Pleim, JE and Hao, JM**. 2014. Impact of aerosol-meteorology interactions on fine particle pollution during China's severe haze episode in January 2013. *Environmental Research Letters* **9**(9). DOI: <https://doi.org/10.1088/1748-9326/9/9/094002>
- Wentworth, GR, Murphy, JG and Sills, DML**. 2015. Impact of lake breezes on ozone and nitrogen oxides in the Greater Toronto Area. *Atmospheric Environment* **109**: 52–60. DOI: <https://doi.org/10.1016/j.atmosenv.2015.03.002>
- Wong, MS, Qin, K, Lian, H, Campbell, JR, Lee, KH and Sheng, SJ**. 2017. Continuous ground-based aerosol Lidar observation during seasonal pollution events at Wuxi, China. *Atmospheric Environment* **154**: 189–199. DOI: <https://doi.org/10.1016/j.atmosenv.2017.01.051>
- Wu, C, Wang, G, Cao, C, Li, J, Li, J, Wu, F, Huang, R, Cao, J, Han, Y, Ge, S, Xie, Y, Xue, G and Wang, X**. 2019. Chemical characteristics of airborne particles in Xi'an, inland China during dust storm episodes: Implications for heterogeneous formation of ammonium nitrate and enhancement of N-deposition. *Environmental Pollution* **244**: 877–884. DOI: <https://doi.org/10.1016/j.envpol.2018.10.019>
- Xiao, H, Carmichael, GR, Durchenwald, J, Thornton, D and Bandy, A**. 1997. Long-range transport of SO_x and dust in East Asia during the PEM B Experiment. *Journal of Geophysical Research-Atmospheres* **102**(D23): 28589–28612. DOI: <https://doi.org/10.1029/96JD03782>
- Yoshitomi, M, Wild, O and Akimoto, H**. 2011. Contributions of regional and intercontinental transport to surface ozone in the Tokyo area. *Atmospheric Chemistry and Physics* **11**(15): 7583–7599. DOI: <https://doi.org/10.5194/acp-11-7583-2011>
- Zhang, WH, Xu, H and Zheng, FJ**. 2018. Aerosol Optical Depth Retrieval over East Asia Using Himawari-8/AHI Data. *Remote Sensing* **10**(1). DOI: <https://doi.org/10.3390/rs10010137>
- Zhang, Y, Sperber, KR and Boyle, JS**. 1997. Climatology and interannual variation of the East Asian winter monsoon: Results from the 1979–95 NCEP/NCAR reanalysis. *Monthly Weather Review* **125**(10): 2605–2619. DOI: [https://doi.org/10.1175/1520-0493\(1997\)125<2605:CAIVOT>2.0.CO;2](https://doi.org/10.1175/1520-0493(1997)125<2605:CAIVOT>2.0.CO;2)
- Zhao, SY, Zhang, H and Xie, B**. 2018. The effects of El Niño-Southern Oscillation on the winter haze pollution of China. *Atmospheric Chemistry and Physics* **18**(3): 1863–1877. DOI: <https://doi.org/10.5194/acp-18-1863-2018>
- Zheng, XY, Fu, YF, Yang, YJ and Liu, GS**. 2015. Impact of atmospheric circulations on aerosol distributions in autumn over eastern China: Observational evidence. *Atmospheric Chemistry and Physics* **15**(21): 12115–12138. DOI: <https://doi.org/10.5194/acp-15-12115-2015>

How to cite this article: Peterson, DA, Hyer, EJ, Han, S-O, Crawford, JH, Park, RJ, Holz, R, Kuehn, RE, Eloranta, E, Knute, C, Jordan, CE and Lefer, BL. 2019. Meteorology influencing springtime air quality, pollution transport, and visibility in Korea. *Elem Sci Anth*, 7: 57. DOI: <https://doi.org/10.1525/elementa.395>

Domain Editor-in-Chief: Detlev Helmig, Institute of Alpine and Arctic Research, University of Colorado Boulder, US

Associate Editor: Md Firoz Khan, Department of Chemistry, Universiti Malaya, MY

Knowledge Domain: Atmospheric Science

Part of an *Elementa* Special Feature: Korea-United States Air Quality (KORUS-AQ)

Submitted: 30 May 2019 **Accepted:** 15 November 2019 **Published:** 27 December 2019

Copyright: © 2019 The Author(s). This is an open-access article distributed under the terms of the Creative Commons Attribution 4.0 International License (CC-BY 4.0), which permits unrestricted use, distribution, and reproduction in any medium, provided the original author and source are credited. See <http://creativecommons.org/licenses/by/4.0/>.